Materials Horizons

ROYAL SOCIETY OF CHEMISTRY

REVIEW

View Article Online
View Journal | View Issue

Cite this: *Mater. Horiz.*, 2024, 11, 3721

ROS-responsive hydrogels: from design and additive manufacturing to biomedical applications

Minju Pu,[ab] Huan Cao,[c] Hengjie Zhang,[b] Tianyou Wang,[b] Yiwen Li,[b] Shimeng Xiao*[a] and Zhipeng Gu *[b]

Received 14th March 2024,
Accepted 16th May 2024

DOI: 10.1039/d4mh00289j

rsc.li/materials-horizons

Hydrogels with intricate 3D networks and high hydrophilicity have qualities resembling those of biological tissues, making them ideal candidates for use as smart biomedical materials. Reactive oxygen species (ROS) responsive hydrogels are an innovative class of smart hydrogels, and are cross-linked by ROS-responsive modules through covalent interactions, coordination interactions, or supramolecular interactions. Due to the introduction of ROS response modules, this class of hydrogels exhibits a sensitive response to the oxidative stress microenvironment existing in organisms. Simultaneously, due to the modularity of the ROS-responsive structure, ROS-responsive hydrogels can be manufactured on a large scale through additive manufacturing. This review will delve into the design, fabrication, and applications of ROS-responsive hydrogels. The main goal is to clarify the chemical principles that govern the response mechanism of these hydrogels, further providing new perspectives and methods for designing responsive hydrogel materials.

Wider impact

Over the years, hydrogels have made impressive advancements in their versatility, performance, and applications. The newest innovation involves smart hydrogels that can adapt their properties to changing environmental conditions. ROS-responsive hydrogels, which can manage irregular ROS levels in living organisms, hold great potential as a treatment option for various diseases. Many hydrogels that respond to ROS have been developed by researchers, and they have shown promising results in animal models. However, creating hydrogel products with high translational properties for clinical use still presents challenges. Thanks to additive manufacturing technology, complex 3D structures with tailored shapes, sizes, and functions for ROS-responsive hydrogels can now be created more easily. This technology has opened up possibilities for various applications ranging from tissue engineering to wearable devices. This comprehensive review introduces the different ROS-responsive structures of ROS-responsive hydrogels and discusses the feasibility of preparing them using additive manufacturing technology. With further development, ROS-responsive hydrogels are poised to expand their applications in fields such as regenerative medicine, advanced materials, and consumer products.

1 Introduction

Hydrogels are three-dimensional networks of cross-linked polymer chains that can swell in water and retain water efficiently.[1,2] Additionally, as soft materials, hydrogels exhibit very similar properties to the extracellular matrix,[3] which makes them ideal materials for biomedical applications, such as drug delivery,[4,5] tissue engineering,[6–8] medical devices,[9–11] antibacterial materials,[12] and other aspects. Traditional hydrogels have long been popular biomedical materials, but they have certain limitations when used in living bodies. Traditional hydrogels do not integrate well with tissue interfaces, and cannot self-adapt their properties based on tissue repair rates. To overcome these challenges, researchers have developed intelligent responsive hydrogels that are highly biocompatible. Due to the introduction of ROS response modules, ROS-responsive hydrogels often have a dual network structure,[13,14] which makes ROS-responsive hydrogels have stronger mechanical properties. At the same time, the phenylboronic acid structure interacts with the amino or hydroxyl groups on the cell surface, and the ferrocene structure interacts with the benzene ring of aromatic amino acids. These forces can significantly enhance the

[a] *Department of Periodontics, State Key Laboratory of Oral Diseases, National Clinical Research Center for Oral Diseases, West China Hospital of Stomatology, Sichuan University, Chengdu, Sichuan 610041, China. E-mail: shimengxiao817@163.com*
[b] *College of Polymer Science and Engineering, State Key Laboratory of Polymer Materials Engineering, Sichuan University, Chengdu, Sichuan 610065, P. R. China. E-mail: guzhipeng2019@scu.edu.cn*
[c] *Laboratory of Clinical Nuclear Medicine, Department of Nuclear Medicine, National Clinical Research Center for Geriatrics, West China Hospital, Sichuan University, Chengdu, 610065, P. R. China*

adhesion ability of hydrogels at biological interfaces.[15,16] Reactive oxygen species (ROS) is a collective term that describes the chemical species formed upon incomplete reduction of oxygen,[17–19] including the superoxide anion ($O_2^{\bullet -}$), hydrogen peroxide (H_2O_2), hydroxyl radicals ($^{\bullet}OH$), and singlet oxygen ($^1O_2$).[20–22] ROS is a signaling molecule that is produced naturally during respiration. It plays a crucial role in regulating various physiological processes across all forms of life.[17,23,24] Generally, oxidative stress resulting from the excessive production of ROS is a common characteristic of various diseases (such as inflammation, cancer, trauma, *etc.*).[25–27] A ROS-responsive hydrogel is a type of intelligent hydrogel that contains multiple modules sensitive to ROS. These modules function as bridges that link the polymer skeleton together utilizing various cross-linking forces such as covalent bond, coordination, and intermolecular forces. When exposed to an oxidative stress environment, the ROS-responsive modules in the hydrogel skeleton are destroyed by oxidation, which results in damage to the integrity of the hydrogel network and causes the gel to undergo either swelling–shrinking or gel–sol transition. In the inflammatory microenvironment of organisms, the adaptive and intelligent behaviors of ROS-responsive hydrogels are observed. In the initial stage of inflammation, where the ROS concentration is high, the ROS response module of hydrogels rapidly scavenges ROS and releases active molecules to alleviate inflammation. As inflammation subsides, the drug release decreases to prevent side effects. Furthermore, by elaborating on designing the composition and structure of ROS-responsive hydrogels, it is possible to link the ROS response with volume, resistance, and other physical and chemical properties of the material, thereby achieving more precise control of the inflammation treatment process.[28] Not only that, the ROS response structure also shows obvious modular characteristics. For a given mature hydrogel, the ROS response module can be used as part of the preparation material to form the hydrogel, and will not have a disruptive impact on the properties of the hydrogel except for the introduction of ROS responsiveness. Simultaneously, most ROS response structures are also highly compatible, and groups or molecules with other different functions can be introduced into the ROS-responsive hydrogels. This modular design makes the ROS-responsive hydrogel more customizable and scalable. Furthermore, the response mechanism of the ROS-responsive hydrogel initiates on the surface, where ROS induces irregular pores to form. Subsequently, the ROS response propagates deeper into the hydrogel as these pores penetrate further.[29] As this layer undergoes a gel–sol transition or swells, the reaction then proceeds deeper into the hydrogel. This outside-to-inside reaction process links the response rate of ROS to the microstructure of the hydrogel's surface. As a result, additive manufacturing technology has become an appealing method for ROS-responsive hydrogel fabrication. By customizing the surface microstructure, this technique enables precise control of the response rate and enhances the reliability of the customization. The reproducibility of this method ensures that the ROS-responsive hydrogel can adapt effectively to complex usage environments. Therefore, the ROS-responsive hydrogel has broad prospects as a raw material for additive manufacturing. In this review, we summarize ROS-responsive hydrogels with various responsive modules, processing methods and applications (Table 1).

2. Hydrogel design from different responsive modules

2.1. Phenylborate and derivatives

Due to the unique structure of boric acid and its derivatives, when reacting with *cis*-α-diols, β-diols, or other compounds, the resulting compound forms a thermodynamically stable ring, and the reaction equilibrium is greatly biased toward the product. It was discovered that polyhydroxy polymers such as poly(glyceryl methacrylate)[77] and polysaccharides[78–80] can form a gel when combined with borax solutions. After conducting NMR analysis of the gels, it was determined that the reaction between boronic acid and *cis*-α-diols or β-diols is the primary factor causing gelation.[81] Organoboric acid compounds exhibits sensitivity to ROS,[82,83] and the response mechanism is succinctly described in Fig. 1(a). The unoccupied 2p orbital in the boron atom allows H_2O_2 to act as a nucleophile. As a result, the lone pair on oxygen in $^{-}O_2H$ initiates a nucleophilic attack, creating intermediate a1. Subsequently, a rearrangement similar to the Baeyer–Villiger reaction generates intermediate a_2, then a_2 rapidly hydrolyzes to the final product b.[84] The rearrangement process is the entire reaction's rate-limiting step.[85,86] Whether it is an aryl boronic acid ester or an alkyl boric acid ester, its ROS responsiveness comes from the rearrangement between the boronic acid group and the oxygen atom of the peroxy bond. It is generally believed that phenylboronic acid can be oxidized under physiological conditions, while the oxidation of alkylboronic acid esters requires a strong alkaline environment.[87] As for boric acid, it does not have the ability to respond to ROS. Usually, the synthesis of phenylboronate requires alkaline conditions and the removal of any produced H_2O to facilitate the forward reaction. It is feasible to quickly form phenylboronate by adjusting the pH of the environment above the pK_a value of phenylboronic acid. In 1949, the first boronic acid-containing hydrogel was synthesized by mixing an alkaline borax solution and polyvinyl alcohol (PVA) solution.[88] The formation of phenylborates depends primarily on the chemical equilibrium of the reaction between phenylboronic acid and diol. Temperature and pH play a decisive role in the reaction, while the sources of the two are insignificant in comparison.[78,89] Since the bond energy of borate ester is low and the reaction is exothermic, heating substantially affects the gelation process.[90] Once a specific temperature reached, the gelation process may even be reversed.[91] Meanwhile, esterification can only happen when the environmental pH is higher than the pK_a of phenylboronic acid.[92] Common phenylboronic acids have a high pK_a value of 8–9, which makes it difficult to create stable hydrogels in physiological environments.[93,94]

Table 1 ROS-responsive hydrogels and their application

	Processing method	Form of material deposition	Application	Ref.
Phenylborate and derivatives	Mould	Shapes form through leaving in a specific container	Self-healing materials	30
			Theoretical research	31
			Drug delivery	32
			Biomimetic materials	33
			Diabetic wound healing	34
	Extrusion	Extrude continuous hydrogel line, or continuous droplets deposited to form line	Colloidal photonic crystals	35
			Bioink	36
			Cell carriers	37
			Dressing	38
			Myocardial damage	39–41
			Cell scaffold	42 and 43
			Wound healing	44
			Patterned hydrogel	45
	Stereolithography (SLA) Light curing	Shapes (line/dot) form through selective curing of photopolymer	Dynamic hydrogel	46
			Tissue repair	47
Ferrocene	Mould	Shapes form through leaving in a specific container	Theranostics	48 and 49
			Drug delivery	50
			Conductive soft material	51
			Glucose sensor	52
			Antibacterial material	53
	Two-photon printing (2PP)	Shapes (line/dot) form through selective curing by 2PP	Nanofabrication	54
Thioketal\thioacetal	Mould	Shapes form through leaving in a specific container	Cell therapy	55
	Extrusion	Extrude continuous hydrogel line, or continuous droplets deposited to form line	Spine cord regeneration	56
			Wound healing	57
			Probiotic therapy	58
			Cartilage repair	59
			Antibacterial material	60
Thioether	Mould	Shapes form through leaving in a specific container	Wound healing	61
			Cell culture and cell therapy	62
	Extrusion	Extrude continuous hydrogel line, or continuous droplets deposited to form a line	Dressing	63 and 64
			Tissue repair	65
	Stereolithography (SLA)	Shapes (line/dot) form through selective curing of a photopolymer	Drug delivery	66
Selenide/telluride	Mould	Shapes form through leaving in a specific container	Stain sensors	67
Diselenide bond	Mould	Shapes form through leaving in a specific container	Drug delivery	68
			H_2O_2/pH sensors	69
			Stain sensors	70 and 71
	Extrusion	Extrude the continuous hydrogel line, or continuous droplets deposited to form line	Dressing	72
			Gel scaffold	73
			Cancer therapy	74 and 75
			Bone repair	76

Many hydrogels based on phenylborates have been developed due to their sensitive response to ROS and rapid gelation process. These hydrogels can be broadly categorized into two types: (1) hydrogels constructed using phenylborates as cross-linking agents, which disintegrate upon response; (2) drugs conjugated with phenylboronic acid, and the drugs are released after response.

Benzoxaborole, a cyclic hemiboronic acid with a lower pK_a value of 7.2, exhibits exceptional binding affinity towards *cis*-diol under neutral pH conditions.[95–97] In the work of Chen *et al.*, an NG-Gal nanogel with a lactose-rich structure was synthesized, which exhibited a particle size of approximately 213 nm.[30] After mixing with poly(DMA-st-MAABO), the solution demonstrated evident gelation at the physiological

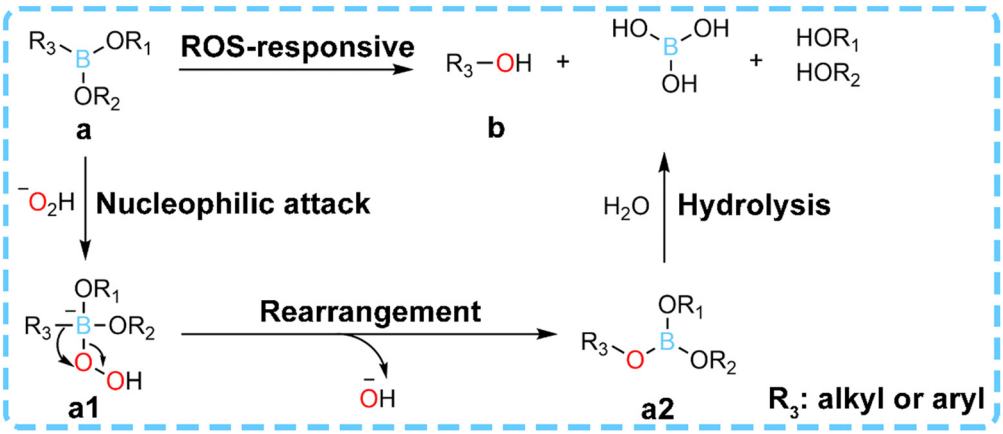

Fig. 1 The response mechanism of phenylboronate to ROS.

pH (7.4). In subsequent experiments, it was observed that increasing the content of the NG-Gal nanogel while fixing the poly(DMA-st-MAABO) content resulted in superior hydrogel mechanical properties (Fig. 2(a)). The porous hydrogel exhibited a high sensitivity toward ROS. In detail, the prepared hydrogel would collapse and fully degrade after being immersed in a 10 mM H_2O_2 solution for 160 minutes. Additionally, introducing electron-withdrawing groups (*i.e.*, fluorine and nitro groups) on benzene is a viable strategy for decreasing the pK_a of phenylboronic acid.[98,99]

Modifying the side chain of a polymer with phenylboronic acid is the most convenient method for constructing phenylboronic-containing hydrogels.[40,100,101] Natural polysaccharides with abundant *cis*-diol are frequently employed as a scaffold for creating phenylboronic acid hydrogels.[43,102,103] Intramolecular or intermolecular cross-linking can be readily achieved by introducing phenylboronic acid groups onto the side chains. In the work of Gao *et al.*, a self-crosslinking hydrogel was developed by hyaluronic acid modified with phenylboronic acid (Fig. 2(b)).[47] Specifically, phenylboronic acid-modified

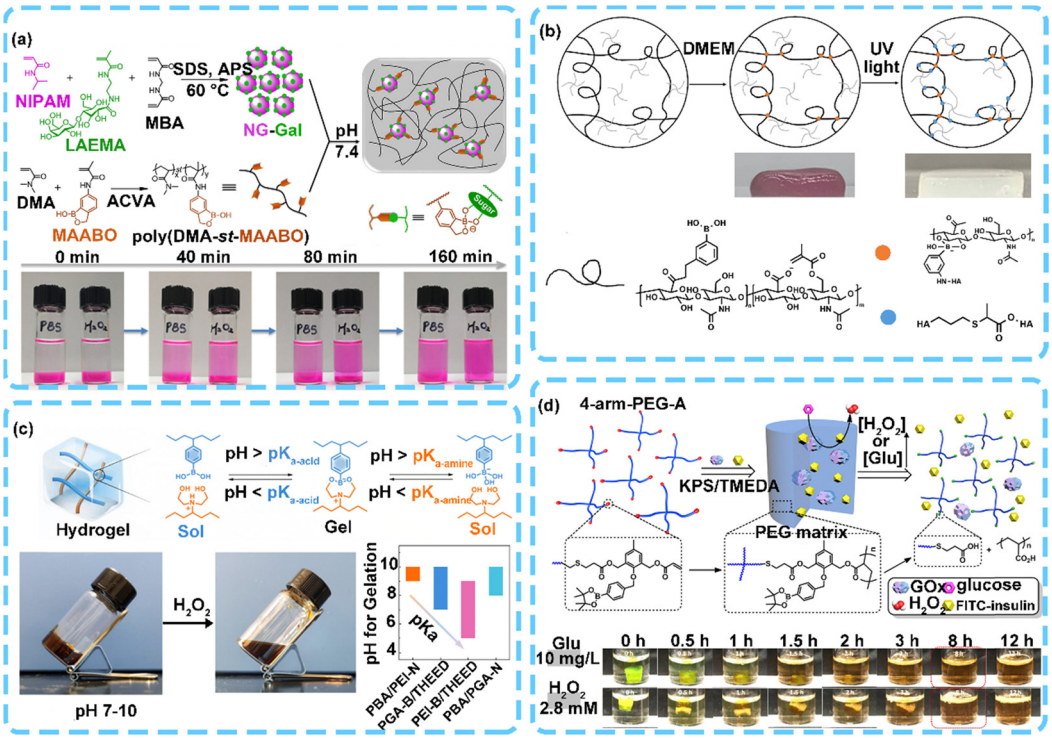

Fig. 2 (a) Schematic illustration of NG-Gal nanogel preparation and its ROS-responsive properties. Reproduced with permission.[14] Copyright 2019, American Chemical Society. (b) Schematic illustration of the reversible crosslinking strategy of PBA microgels and its decomposition–recombination ability. Reproduced with permission.[12] Copyright 2021, Elsevier. (c) Schematic formation of different IBNCB hydrogels at different pHs and its ROS-responsive behavior. Reproduced with permission.[13] Copyright 2023, American Chemical Society. (d) Preparation and ROS-/Glu-responsive degradation of hydrogel. Reproduced with permission.[17] Copyright 2017, American Chemical Society.

HA–MA–PBA with varying polymer weight percentages (1, 2, and 3 wt%) and sulfhydryl-functionalized four-arm PEG was dissolved in a high-sugar DMEM medium to obtain a single cross-linked hydrogel (SC gel). A doubly crosslinking hydrogel (DC gels) was generated by further photo-initiated crosslinking. It also showed satisfactory antioxidant activity with a scavenging rate of 58.38% for HA–MA–PBA in the measurement of free radical scavenging. Furthermore, Zhou *et al.* constructed a triple dynamically cross-linked hydrogel containing Schiff base bonds, phenylborate, and hydrogen bonds through the blending of PBA grafted PLL (PP), oxidized dextran (OD), and SeNPs.[33] The OD-PP@SeNPs hydrogel has ideal mechanical and adhesion properties. It showed significant degradation in a simulated oxidative environment *in vitro*. Additionally, Kang *et al.*[31] developed an internal boron–nitrogen coordinated boronic ester (IBNCB) hydrogel with a lower gelation pH and ROS-responsive capabilities (Fig. 2(c)). The designing and constructing of the IBNCB hydrogel based on internal coordination between boron and nitrogen can be modulated by varying polymers with phenylboronic acid or *N*,*N*-bis (2-hydroxyethyl) moieties, such as PGA-B and THEED. IBNCB hydrogels exhibit a lower pH threshold for gelation than phenylboronic acid hydrogels at room temperature and 37 °C. Competition tests demonstrated that phenylboronic acid showed a greater propensity to generate IBNCB with *n*-methyldiethanolamine (MDEA) under identical conditions, and its equilibrium constant ($K_{\text{eq-IBNCB}}$: 246.67 M) was significantly higher than that of conventional boronate ($K_{\text{eq-1,2 }o\text{-diol phenylboronic acid ester}}$: 3.31 M) according to further calculations, which confers enhanced stability upon IBNCB hydrogels relative to traditional borate hydrogels at physiological pH. Furthermore, the utilization of PEI enables the formation of a PEI-B/THEED hydrogel even under acidic conditions with pH as low as 5.

Telechelic polymers are a class of polymers with reactive groups present in monomers at the end of the chains.[104–106] Due to their unique structure, telechelic polymers are frequently used to construct 3D network structures.[107–109] For instance, Zhang *et al.* developed a ROS-responsive hydrogel from 4-arm-PEG-AD as an insulin delivery system (Fig. 2(d)).[32] By encapsulating glucose oxidase (GOx) that catalyzes the oxidation reaction of glucose to generate H_2O_2 and trigger the ROS-responsivness of phenylborate, the hydrogel was endowed with glucose responsiveness which could control insulin release. Meanwhile, Due to the sensitivity of hydrogels to ROS, only a small amount of GOx (0.001 wt% of dry gel) can trigger the oxidative degradation of hydrogels, and the glucose-oxidation process was not influenced by other carbohydrates in the body. A hydrogel loaded with FITC-insulin showed a clear process of swelling and dissolving when being incubated in a glucose or H_2O_2 environment. It was also noticed that as the concentration of H_2O_2 increased, the degradation rate of the hydrogel increased further.

2.2. Ferrocene

Ferrocene (Fc) is an exemplary organometallic complex with exceptional stability and redox properties, due to its stable 18-electron configuration.[110] The presence of iron ions causes Fc to exhibit varying oxidation states and undergo changes in its spatial configuration as its valence state changes.[111–113] It can form cationic ferricenium species and causes the angle between the two cyclopentadienyl anions to gradually increase (Fig. 3(a)), while also increasing hydrophilicity and reducing the ability to combine with host macromolecules.[114] Another characteristic of ferrocene is that it can be used as a guest molecule to form stable inclusion compounds with hosts such as cyclodextrin.[115] These inclusion compounds can rapidly decompose due to the spatial configuration change of Fc after oxidation.[116,117] Fc-containing hydrogels can be divided into two groups based on the main forces present in the hydrogel: (1) covalently cross-linked Fc-containing hydrogels; and (2) supramolecular Fc-containing hydrogels (Fig. 3(b)). In the covalently cross-linked group, Fc causes a significant increase in hydrophilicity within the hydrogel due to the oxidation response. These changes are observed macroscopically as alterations in the volume and rheological properties of the hydrogel. In supramolecular Fc-containing hydrogels, the host–guest interaction quickly disappears with the oxidation of Fc, which leads to the hydrogels transforming from gel to sol macroscopically.

Covalently cross-linked hydrogels are typically characterized by forming 3D networks through irreversible covalent bonding between polymer chains.[118,119] This method of production gives the hydrogels exceptional stability and excellent mechanical strength.[120] Poly(ferrocenylsilanes) (PFSs), prepared by ring-opening polymerization of silicon-bridged [1]ferrocenophanes, is commonly used to prepare chemically cross-linked Fc-containing hydrogels.[121–123] By modifying silane further, reactive groups can be introduced into the side chain resulting in the formation of PFS hydrogels. These hydrogels contain a high density of Fc units within the networks, which makes them highly responsive to external redox changes. Zhang *et al.* have developed a dual-responsive PFS hydrogel using hysteretic volume-phase transition (Fig. 4(a)).[51] By carefully controlling the reaction conditions, it is possible to achieve accurate control over the degree of crosslinking (x) and the DMAPMA/PBu3 ratio ($(x + y):z$). By adjusting the ambient temperature and redox state of hydrogels, the volume can be regulated reversibly. The addition of Fc to the polymer side chain greatly simplifies the synthesis process and maintains its redox responsiveness. In the study reported by Gu and colleagues, Fc exhibits reduction capabilities towards Ag(I), resulting in the formation of metal nanoparticles, while triazole coordinates with them to generate stable AgNPs (Fig. 4(b)).[53] The difference between the hydrogels obtained by different preparation methods is revealed by further analysis using differential scanning calorimetry (DSC). A direct blending of gelatin P(NCHO-*b*-NFc-*b*-NTEG-*b*-NCHO) and $AgNO_3$ caused a higher value of transition temperature (T_g) and enthalpy changes (ΔH), which can be attributed to the uniform distribution of AgNPs. In contrast, immersing the hydrogel in the AgNPs solution induces relaxation of macromolecular chains, resulting in uneven distribution of AgNPs within the hydrogel. Both factors contribute to the instability of the hydrogel, particularly in AgNPs-HG-3.

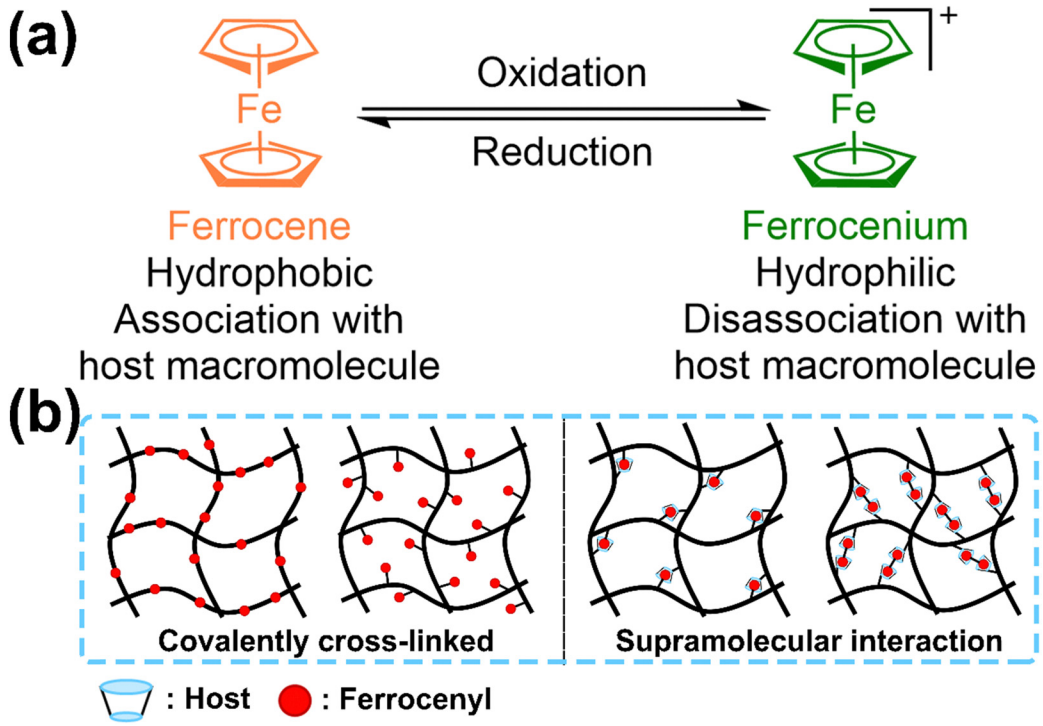

Fig. 3 (a) The mutual transformation of ferrocene and ferrocenium. (b) Schematic structures of covalently cross-linked and supramolecular Fc-containing hydrogels.

Supramolecular hydrogels are highly organized systems across length scales whose formation is dependent upon dynamic non-covalent bonds such as host–guest interactions, hydrogen bonding, and coordination. These hydrogels are highly responsive to changes in their environment and can simulate organisms due to their dynamic reversibility.[124,125] As a guest molecule, Fc can form stable inclusion compounds with host molecules like β-CD and pillararenes[6]. These inclusion compounds break down quickly when Fc oxidizes into ferrocenium ions, which is useful in creating supramolecular hydrogels that respond to ROS. Jain and colleagues developed a glucose sensor utilizing the redox capability of Fc.[52] The enzyme-fuel pairs horseradish peroxidase (HRP)-H_2O_2 (oxidant fuel) and glucose oxidase (GOx)-D-glucose (reduced fuel) were responsible for governing the redox response behavior. These pairs showed self-regulating behavior that was dependent on the concentration of D-glucose supplied to the chemical reaction network. In Fig. 4(c), it is shown that HRP and H_2O_2 can oxidize Fc in the gel sensor, causing it to break down and turn into a solution. But, when GOx and D-glucose were added to create a reducing environment, the solution reassembled back into a gel quickly. If there is an excess of D-glucose in the hydrogel environment, the enzymatic intermediate GOx[FADH2] will lose its reducing properties and produce H_2O_2, which causes the hydrogel network to shift from an equilibrium-responsive state to a non-equilibrium self-regulating state. This results in autonomous assembly and disassembly of the hydrogel at different concentrations of D-glucose. Similarly, Ni *et al.* prepared a series of intelligent Fc-containing hydrogels (G1a–e with different molar ratios of Fc).[50] When hydrogels were placed in a water-soluble pillar[6]arene (WP6) solution for a specific time, their mass increased to varying degrees through the interaction between Fc and WP6 through host–guest binding (Fig. 4(d)). However, due to the hydrophobicity of Fc, the hydrogels become less able to absorb water as the molar ratio of Fc increases. When placed in an aqueous solution of WP6, the swelling ratio initially increases between Fc molar proportions of 0% to 10% before decreasing between Fc molar proportions of 10% to 20%. Furthermore, the diameter of G1c/WP6 decreased from 35 mm to 20 mm under the oxidation of $AgNO_3$, but the use of hydrazine hydrated water solution gradually restored the diameter of G1c/WP6 to 28 mm. The same disposal occurred with G1c, but with opposite results. This phenomenon due to the ferrocenium ion with a positive charge strengthened the host–guest interaction with the negatively charged WP6. This created a pseudo zwitterionic polymer, which caused the volume of the hydrogel to decrease macroscopically. Conversely, the process of swelling behavior in G1c contributed to the transition from hydrophobic to hydrophilic Fc. This resulted in electrostatic repulsion between positively charged ferrocenium ions.

2.3. Sulphur derivatives

Thioacetal/thioketal was previously used to protect ketone/aldehyde from being destroyed, while thioethers were commonly used as reducing agents or antioxidants. However, with the advancements in materials science, the ROS-responsive characteristics of these two groups have been increasingly recognized.[126–128] In ROS-responsive hydrogels, they are often used as cross-linking points to aid in the construction of the hydrogel. The response mechanism of thioketal/thioacetal to

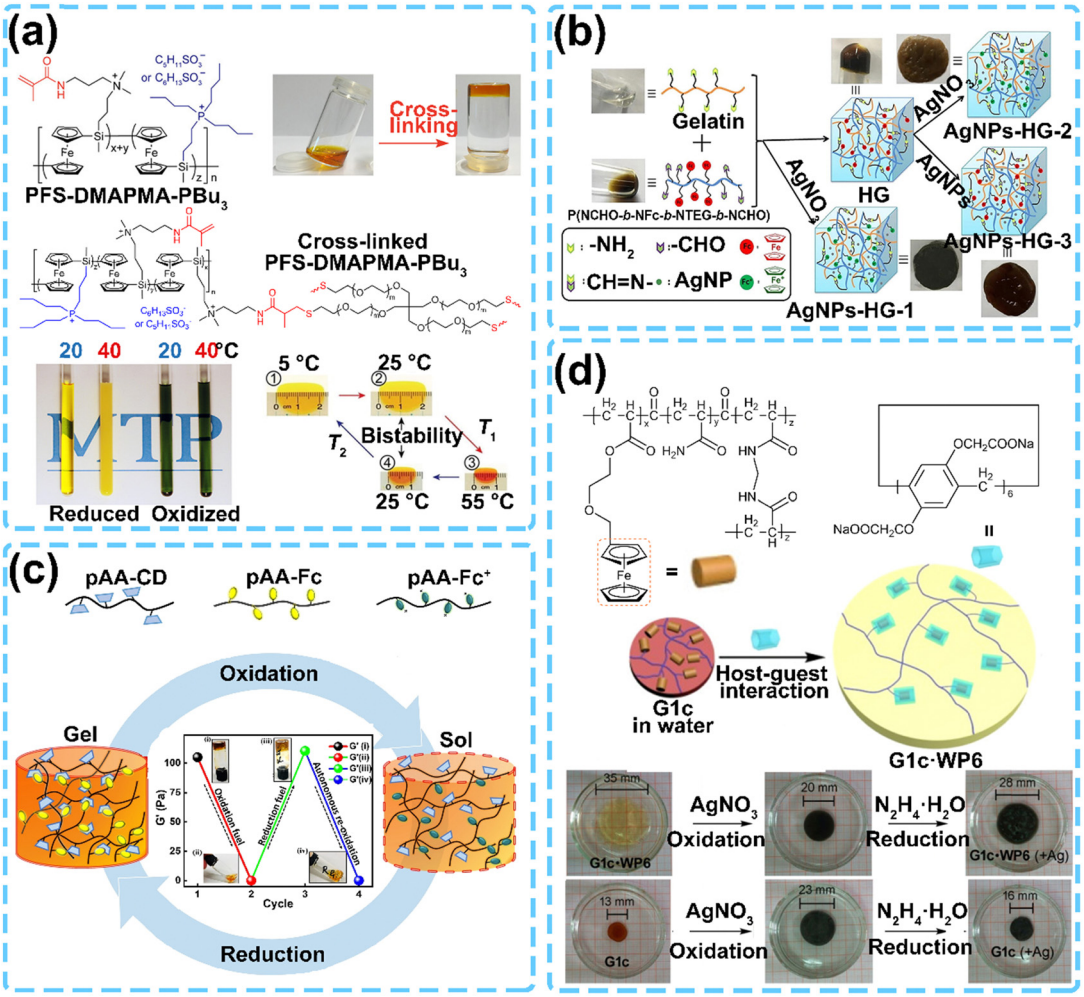

Fig. 4 (a) Preparation of PFS-based hydrogel and its responsiveness. (b) Different preparation methods and properties of hydrogels with Fc modified side chain. Reproduced with permission.[34] Copyright 2019, Elsevier. (c) Fuel-driven redox-responsive hydrogel with autonomous assembly and disassembly capabilities in the presence of D-glucose. Reproduced with permission.[33] Copyright 2017, Wiley-VCH. (d) Schematic illustration of the redox response of supramolecular hydrogels and volume changes in oxidizing and reducing environments. Reproduced with permission.[31] Copyright 2016, American Chemical Society.

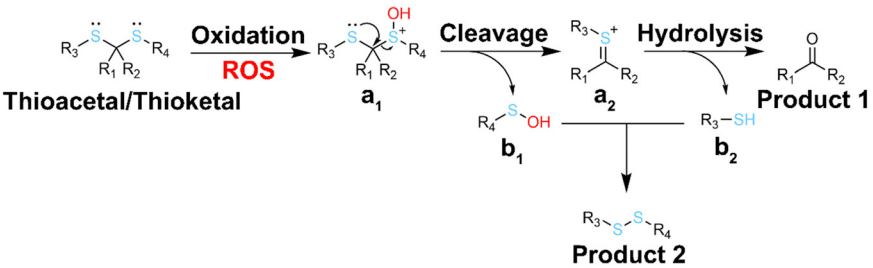

Fig. 5 The response mechanism of thioacetal/thioketal to ROS.

ROS can be described as follows[129] (Fig. 5). At the beginning, ROS, such as H_2O_2, attack the lone pair of sulfur in thioketal/thioacetal, forming intermediate a_1. Then, a_1 undergoes a simple rearrangement, producing intermediate a_2 and intermediate product b_1. Afterward, a_2 is hydrolyzed, resulting in the formation of product 1 and intermediate product b_2. Finally, the two intermediates combine to generate product 2. It is important to note that thiol-containing compounds, like reduced glutathione and methionine, react with the two intermediate products *in vivo*, forming different products. It can be difficult to introduce thioacetal/thioketal simultaneously without experiencing side reactions such as oxidative coupling, due

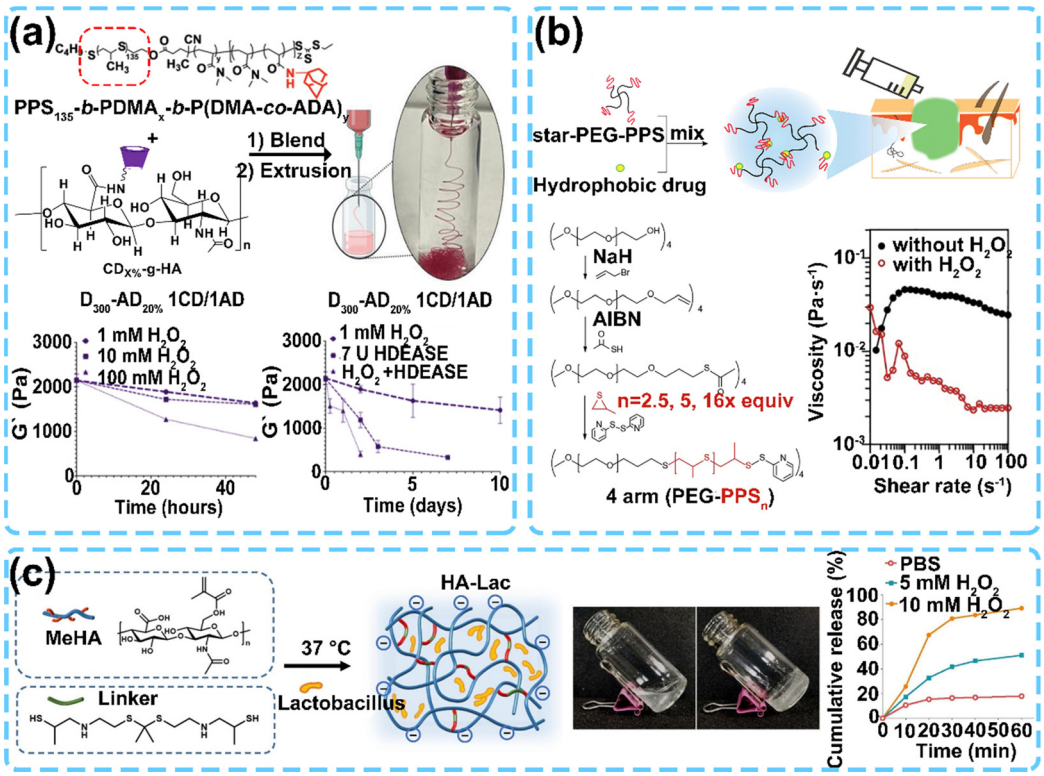

Fig. 6 (a) Synthesis schemes for the PEG–MAL–PTK macromer and the gel swelling ratio under different conditions. Reproduced with permission.[46] Copyright 2023, Wiley-VCH. (b) Phase transition of different molecular weight star-PEG-PPS in different solvents and viscosity change in response to ROS. Reproduced with permission.[85] Copyright 2018, Elsevier. (c) Preparation, rheology properties, and ROS-responsive ability of HA-Lac. Reproduced with permission.[37] Copyright 2022, Elsevier.

to the high reactivity of sulfhydryl during the hydrogel formation process. However, there are two promising solutions: constructing polymers that contain thioacetal/thioketal in the backbone or utilizing small molecule crosslinkers with thioacetal/thioketal (Fig. 6(a)).

In the study of Martin *et al.*, a ROS-degradable polythione (PTK)-crosslinked PEG hydrogel (PEG–MAL–PTK) was prepared and utilized as an antioxidant and cell-degradable platform for stem cell delivery.[55] To evaluate the ROS-responsive ability and degradation *in vitro* of these hydrogels, 7.5 wt% hydrogels made of non-responsive PEG-dt and responsive PEG–MAL–PTK were incubated in a medium with different concentrations of H_2O_2. When treated with H_2O_2, the PTK hydrogels that were responsive to ROS showed a more significant increase in swelling compared to the PEG-dt hydrogels. Analogously, in the study of Huang *et al.*, a ROS-responsive hydrogel was developed through Michael addition between small molecules containing thioketals with thiol at both ends as crosslinkers, and methacrylic acid-modified hyaluronic acid (MeHA) (Fig. 6(c)).[58] To test the release of probiotics, hydrogels were incubated in different environments. A burst and continuous release of encapsulated bacteria occurred when triggered by H_2O_2. The rate of release increased with H_2O_2 concentration, with approximately 90% of bacteria being released after incubation with 10 mM H_2O_2 for 60 minutes. These results suggest that the hydrogel can be utilized as a responsive platform for delivering probiotics and controlling their release in response to ROS.

Thioethers exhibit high reducing activity. Upon exposure to ROS, they may be converted into sulfoxides or sulfones, which have a greater affinity to water.[130,131] In the study of Zhu *et al.*, an amphiphilic self-assembled star-shaped block copolymer star-PEG-PPS$_n$ was synthesized (Fig. 6(b)).[132] The hydrogel's ROS responsiveness is attributed to PPS. The oxidation-responsive properties of thioethers allow hydrogels to generate sulfoxides or sulfones under the action of ROS, which was verified by detecting the viscosity changes of hydrogels in oxidizing and non-oxidizing environments. Hydrogel underwent oxidation dissolution in the presence of hydrogen peroxide, decreasing the viscosity of the polymeric network. Additionally, in the work of Mariah and coworkers, a nanoparticle (NP) supra-assembly hydrogel was synthesized (Fig. 6(a)).[65] Firstly, nanoparticles were synthesized that contain a thioether structure responsive to ROS inside, and an outer layer rich in the adamantyl structure. These nanoparticles can be mixed with cyclodextrin-modified hyaluronic acid to produce a hydrogel that is sensitive to both ROS and enzymes, acting as a glue.

2.4. Selenide/telluride and the diselenide bond

As chalcogen, selenium and tellurium can replace oxygen to form selenide and telluride, which can be oxidized into selenoxide/telluroxide or further selenone/tellurone with ROS

(such as H_2O_2).[133,134] However, only a few studies have focused on single selenide/telluride as a responsive module to reactive oxygen species (ROS). Researchers typically consider selenide/telluride as a component of a larger system and assess the feasibility of the entire system as a ROS-responsive module. For example, when selenide is oxidized into selenoxide, the β-seleno-dicarbonyl (or β-telluro-dicarbonyl) compound can undergo Ei elimination to produce the α,β-unsaturated carbonyl compound and selenenic acid (or telluric acid) if the compound contains β-carbonyl (Fig. 7(a)),[135] leading to the degradation process of the hydrogel. Furthermore, due to the low electronegativity of selenide and telluride, they can act as electron donors in a configuration that could result in ligands with rich coordination chemistry forming various complexes.[136] In the research of Li *et al.*, a ROS-responsive hydrogel was reported, which could be redox-modulated through dynamic coordination between telluride and metal ion Pt(IV) (Fig. 7(c)).[137] When telluride underwent oxidation (for example, with H_2O_2), the coordination between telluride and Pt(IV) might be disturbed, leading to the release of free Pt(IV). Nevertheless, this coordination interaction could be easily restored by reducing oxidized telluride with vitamin C (VC). Hydrogels without Pt(IV) were prepared by the copolymerization of *N*,*N*′-(tellurobis(propane-3,1-diyl))bis(2-methylacryl-amide) (Acry2-Te) and *N*-hydroxyethylacrylamide (HEMAA) with varying ratios (1 : 10, 1 : 20, and 1 : 40; named hydrogel-10, hydrogel-20, and hydrogel-40). The microstructure and pore size of the hydrogels were significantly impacted by the composition of Acry2-Te to HEMAA, where an increased HEMAA proportion would result in larger pore sizes. Upon introducing Pt(IV) into these hydrogels, there was a noticeable reduction in the pore size for hydrogel-10 and hydrogel-20, while the microstructure of hydrogel-40 remained almost unchanged. After the addition of 50 mM H_2O_2, the pore size significantly increased due to the dissociation of coordination complexes and a decrease in cross-linking density. By introducing Pt(IV) through coordination interactions between Acry2-Te and Pt(IV), the hydrogel's mechanical strength was significantly improved. However, the mechanical strength decreased when Acry2-Te was oxidized by H_2O_2 due to the disintegration of coordination interactions. On the other hand, the mechanical strength could be restored by adding VC, which reduced telluroxide to telluride, thereby reinstating coordination between Te and Pt(IV). Selenium can also form diselenide bonds (Se–Se) which is similar to disulfide bonds (S–S). However, the bond energy of Se–Se (172 kJ mol^{-1}) is considerably lower than that of S–S (251 kJ mol^{-1}).[138] As a result, S–S only undergoes oxidation to sulfoxides or further sulfones under the influence of ROS without any bond cleavage, while Se–Se breaks down rapidly. Therefore, the response to ROS can cause Se–Se to break easily at various inflammatory sites.[139,140] Although some 111 compounds with special disulfide bond structures, such as lipoic acid, are widely recognized as efficient antioxidants, disulfide bonds are more commonly used as a reversible reduction-responsive chemical linkage. When the disulfide bond is exposed to reducing agents like reduced glutathione, it breaks down into two sulfhydryl groups. These sulfhydryl groups can then be used to restore the structure of the disulfide bond when exposed to oxidants like H_2O_2. In the study conducted by Lu *et al.*, an easy-to-peel ROS-responsive smart dressing was developed (Fig. 7(b)).[72] To put it simply, PEtOx was modified by consuming some propionyl groups through hydrolysis. Then, γ-butyroselenolactone was used to treat the remaining amino groups, resulting in the introduction of selenium hydroxyl groups into the side chain, creating PEtOx–EI–SeH. Finally, selenol was crosslinked under air or H_2O_2 conditions in stoichiometric amounts, forming PEtOx–EI–Se_2 hydrogels in just 5 seconds. The PEtOx–EI–Se_2 hydrogel can be dissolved by adding an excess of hydrogen peroxide (a commercial solution of 3 wt% H_2O_2 for medical use) for 15 minutes, which provides a viable option for removing burn wound dressings without causing any tissue damage.

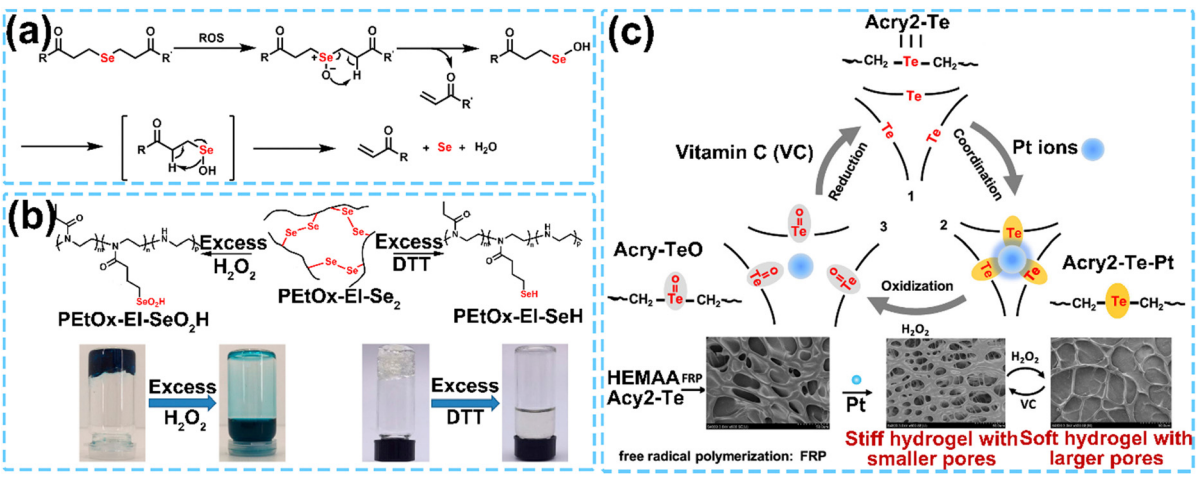

Fig. 7 (a) The degradation mechanism of β-seleno-dicarbonyl within ROS. (b) Dissolution of the hydrogel relies on the oxidation or reduction of diselenide bonds by H_2O_2 or DTT. Reproduced with permission.[48] Copyright 2020, American Chemical Society. (c) Schematic illustration of redox-mediated dynamic coordination between telluroether and Pt(IV) ions. Reproduced with permission.[47] Copyright 2020, American Chemical Society.

2.5. Other moieties

Along with the previously mentioned ROS response components, there are others that have not been studied as extensively, including poly(deca-4,6-diynedioic acid),[141] dopamine,[142,143] polyphenol,[144–146] *etc.* In the work of Zhang and colleagues,[141] a ROS-responsive polymer poly(deca-4,6-diynedioic acid) (PDDA) was creatively constructed and combined with Pullulan to create a ROS-responsive hydrogel PPG (Fig. 8(a)). PDDA could decompose under the influence of ROS and produce highly biocompatible succinic acid. During the whole degradation process, the Raman signal of PDDA (original strength 2121 cm^{-1}) weakens over time with the increasing degree of degradation. Therefore, the relationship between the Raman signal of PDDA and its level of degradation allows researchers to accurately track the hydrogel's decomposition process by observing changes in its Raman signal. In addition, in the study of Li *et al.*, a supramolecular hydrogel composed of DNA/bipyridinium dithienylethene was prepared.[147] In brief, a carboxymethyl cellulose (CMC)-dopamine/DTE_c hydrogel (hydrogel I) was synthesized *via* donor–acceptor interactions between light-responsive small molecule DTE_c and dopamine within dopamine-modified carboxymethyl cellulose. Based on this, short-chain single-stranded nucleic acids were incorporated into the hydrogel to fabricate shape-memory and self-healing matrices (hydrogel IV) (Fig. 8(b)). The shape transformation of hydrogel IV can be precisely regulated by modulating the donor–acceptor interactions between DTE and dopamine through external stimuli (such as light or oxidation/reduction). Under the oxidation of sodium persulfate (1 M, 10 μL, 5 min), the fluidity of the triangular prism-shaped hydrogel IV was significantly enhanced, resulting in the loss of its original geometry. However, the quasi-liquid state hydrogel VI can quickly return to the previous triangular prism shape with ascorbic acid reduction (1 M, 10 μL, 5 min). The effect of light on the as-prepared hydrogel's properties is similar to the impact of oxidation/reduction. At room temperature, hydrogel IV exhibited a shape memory function that could be cycled at least 6 times without significantly altering its shape characteristics. Such stimuli-responsive hydrogels could be used as actuators, sensors, or robotic devices.

3. Additive manufacturing technology for hydrogel fabrication

There are extensive applications of hydrogels in diverse fields, such as biomedical materials,[148–150] bioengineering,[151] smart devices,[152] and soft robotics.[153] With the advancement of synthetic chemistry, the primary obstacle in the development of a ROS-responsive hydrogel is no longer the synthesis or fabrication of such materials. One of the new challenges is achieving precise regulation of the ROS-responsive hydrogel degradation process, to respond to the complex behavioral characteristics of ROS levels under normal and pathological physiological conditions.[154,155] Additionally, developing ROS-responsive hydrogels that can differentiate between normal levels of ROS required for cell function and those that result in elevated levels of ROS due to disease states is a significant challenge.[156] For normal tissues, removing excess ROS could

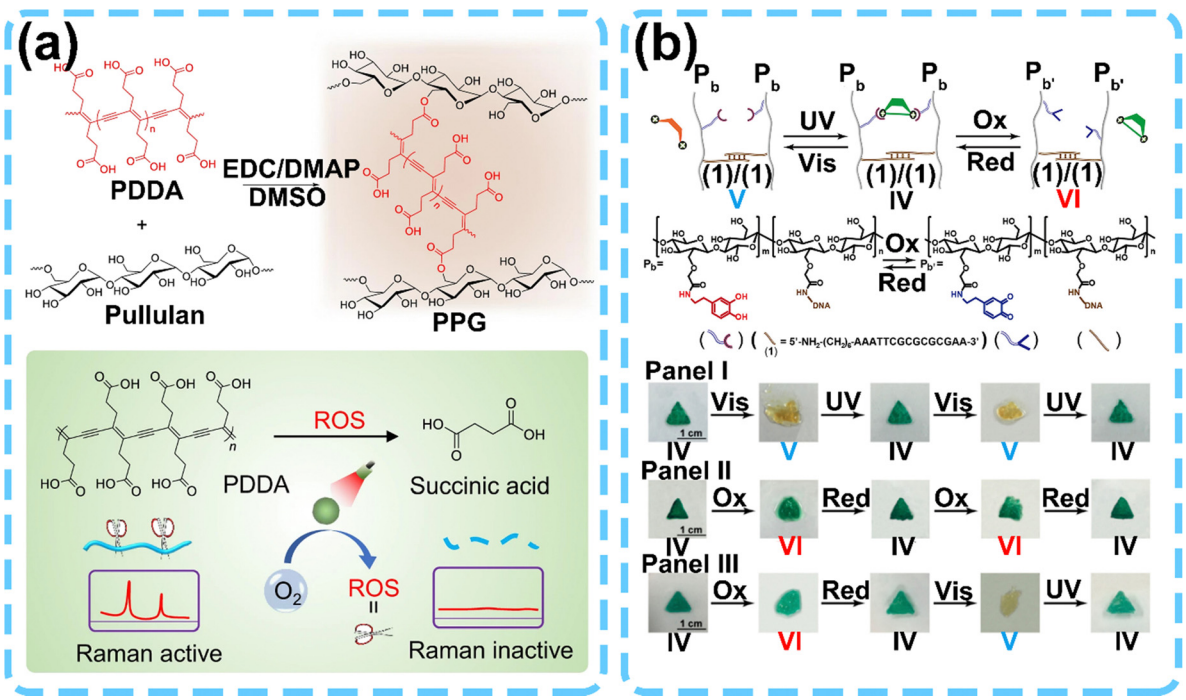

Fig. 8 (a) Preparation of PPG and schematic illustration of PDDA chemical structure and its Raman-traceable, ROS-responsive degradation. (b) Schematic images of the formation and disassembly of the carboxymethyl cellulose hydrogel and representative images corresponding to the shape-memory properties of the hydrogel. Reproduced with permission.[96] Copyright 2018, American Chemical Society.

lead to decreased immunity and obstruct normal metabolic processes, whereas low clearance rates fail to achieve the desired effect for tissues of pathological changes. Ultimately, these all involve regulating the response rate of ROS-responsive materials. For ROS-responsive hydrogels, the reaction between ROS-responsive modules and ROS usually first occurs on the surface of the hydrogels, and then proceeds to penetrate deeper into the hydrogel, causing it to either transition from gel to sol or swell.[157] Although computer simulations can illustrate the interactions between the topological structure on the surface and the response speed of hydrogels,[158] efficiently regulating these interactions to achieve a beneficial outcome poses a significant obstacle.

Additive manufacturing (AM) technology can create complex geometries from computer-aided design (CAD) models, and the process is highly repeatable.[159–161] Currently, building special topological structures on the surface of materials through AM is a mature way to modify the surface of materials, especially in the field of bionics.[162] By building some biologically evolved complex structures on the surface of materials, unique interface functions including superhydrophobicity,[163] drag force reduction,[164] and anisotropic liquid transport[165] have been achieved. Meanwhile, AM technology has good compatibility with ROS-responsive hydrogels,[166] which do not affect the responsiveness of ROS-responsive hydrogels (Fig. 9(d) and (e)).[37,167] The fabrication of hydrogels through AM technology has been extensively researched. However, the development of ROS-responsive hydrogels through this technology is still lacking due to the absence of systematic studies on the compatibility between ROS response modules and various additive manufacturing technologies.

Although numerous excellent reviews have provided detailed introductions to AM technologies and their application,[168,169] there are few reports on the use of AM technologies in the fabrication of ROS-responsive hydrogels. Therefore, this section provides a brief overview of several AM technologies that could be utilized for hydrogel manufacturing, focusing on the feasibility of fabricating ROS-responsive hydrogels using various ROS-responsive modules.

3.1. Laser-based fabrication technology

3.1.1. Stereolithography technology. Stereolithography (SLA), developed by Melchels *et al.* in 1986, is widely recognized as the first commercial AM technology.[170] As shown in Fig. 9(a), an SLA apparatus comprises a laser source with a system for controlling horizontal movement (*XY*-movement), a fabrication platform capable of vertical direction on the *Z*-axis, and a vat for photosensitive resin. During the fabrication process, the photosensitive resin undergoes laser irradiation, which triggers polymerization and solidification from point to line, ultimately

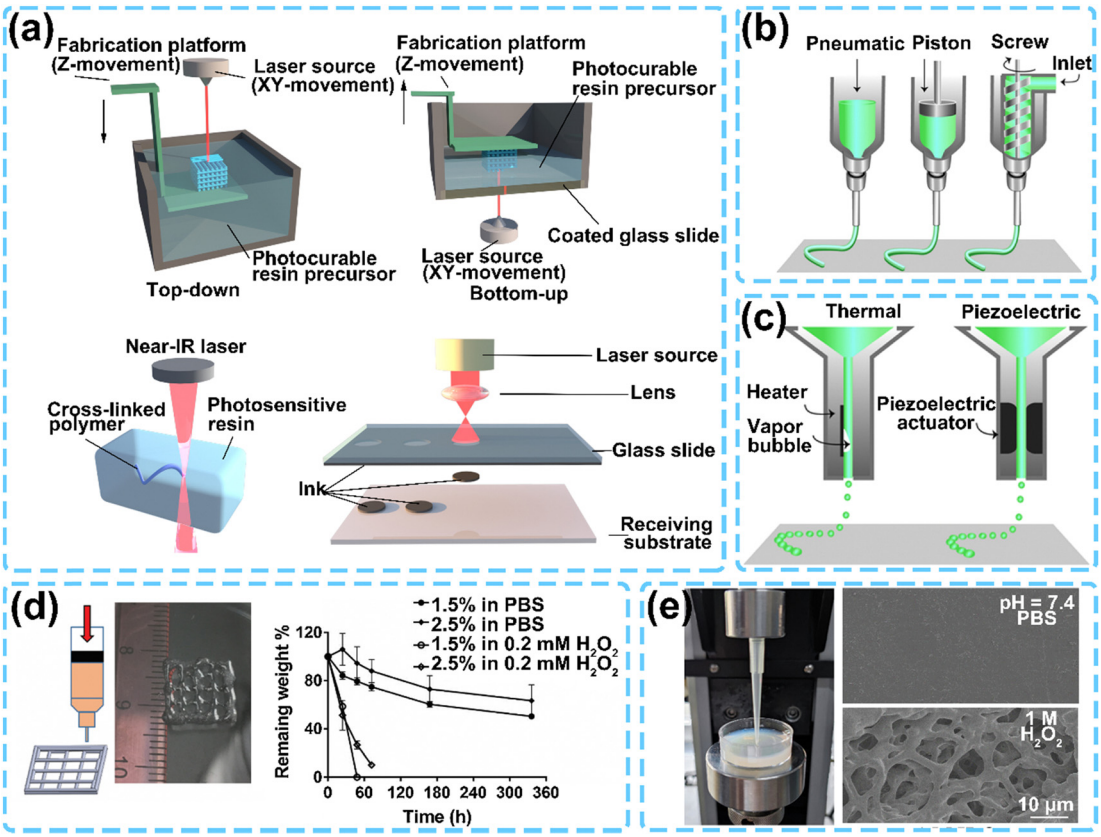

Fig. 9 (a) Laser-based fabrication technology, (b) extrusion-based fabrication technology, and (c) inkjet-based fabrication technology. Reproduced with permission.[113] Copyright 2013, Wiley-VCH. (d) and (e) Fabrication of ROS-responsive hydrogels and their ROS-responsive ability. (d) Reproduced with permission.[18] Copyright 2020, Elsevier. (e) Reproduced with permission.[111] Copyright 2022, Elsevier.

resulting in a complete surface formation. Once a layer is cured, the working platform vertically moves a layer thickness, and the laser proceeds to scan the next layer, the essence of which is a layer-by-layer printing technology. Finally, all the layers are firmly glued together to form the expected 3D model. It is essential to notice that the completed model must be washed to remove excess resin from surfaces. According to the mobile mode of the manufacturing platform, SLA can be classified into two categories: top-down and bottom-up.[170] In the work of Tsai and co-workers,[171] a hydrogel containing phenylborate was used as ink for SLA to create vascularized constructs (Fig. 10(a)). Briefly, the channels in the target structure are first constructed through a sacrificial hydrogel, and then the main structure is obtained by photo-curing the hydrogel containing the phenylboronic acid structure. The target structure is obtained after removing the sacrificial hydrogel.

3.1.2. Two-photon polymerization. Two-photon polymerization (2PP) is an AM technique based on two-photon absorption (2PA) to induce local cross-linking of photopolymers (Fig. 9(a)). As a non-linear absorption process, there is a simultaneous absorption of two photons with identical or different frequencies of 2PA to excite a molecule from the ground state to the excited state.[172] Based on 2PA, 2PP can employ a focused near-infrared laser with lower photon energy, less attenuation, and greater penetration to induce polymerization. The nature of nonlinear excitation can ensure that the polymerization is limited in a narrow space near the focal spot. In 2001, Kawata *et al.* fabricated a 10 μm high and 7 μm long model cow by 2PP with a resolution of 150 nm (approaching the diffraction limit of light), a milestone of 2PP print technology.[173] In the work of Jeske *et al.*,[174] two-photon polymerization was performed on a stoichiometric mixture of PETMP and TTT as shown in Fig. 10(b). Then under the nonlinear absorption of the photoinitiator, the thiol–ene reaction is initiated. Then a curable resin containing a large amount of thioether and having shape-memory behavior for 4D responsive metamaterials was developed. Printed products using this resin exhibit mechanical properties comparable to those of commercial SLA resin-printed products.

3.1.3. Laser-induced forward transfer technology. Laser-induced forward transfer (LIFT) technology is a non-contact printing technique based on the interaction between the laser and ink materials.[175] As shown in Fig. 9(a), the LIFT system consists of three essential components: a laser source, a donor substrate (an optically transparent support film coated with ink materials on the side facing the receiving substrate), and a receiving substrate. When a laser beam is directed onto ink materials (such as metal or hydrogel) through a transparent substrate, a conversion of light energy into internal energy occurs in the ink material at the site with irradiation, resulting in a swift deformation of the ink material and further transfer to the receiving substrate.[176] Mitu *et al.* conducted a study in which they used a silicon dioxide base layer with a deposited ferrocene film for printing through laser-induced forward transfer.[177] With this method, it was possible to quickly create ferrocene thin film pixels and lines onto flexible PDMS substrates without the need for any additional photolithography processes.

3.2. Extrusion-based fabrication technology

Direct ink writing (DIW) technology is the most representative and standard extrusion-based AM technology. It originated from the robocasting (or robotic deposition) technology proposed by J. Cesarano *et al.* in 1998.[178] DIW is now widely used in microelectronics, photovoltaics, energy, tissue engineering, and other fields. For this method, ink is generally inserted in syringes and dispensed on a fabrication platform with the drive of either a pneumatic piston or a screw (Fig. 9(b)). Compared to other AM technologies, the minimum printing unit of DIW is a hydrogel strand, which requires the hydrogel to have a viscidity to maintain the shape of the constructs after printing. In the work of Hery *et al.*, a hydrogel system

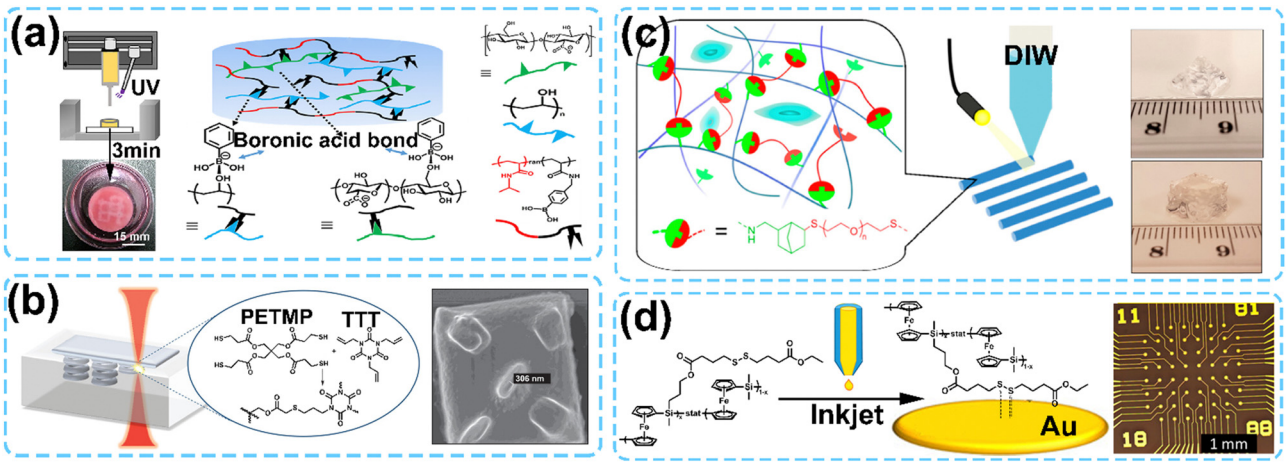

Fig. 10 (a) Schematic of the fabrication process of bulk gel and its main forces. (b) Schematic of 2PP of thiol–vinyl resins to form shape-memory microstructures and entity. (c) Schematic overview of photoactive alginate bioink (Alg-norb) for bioprinting and printed products. (d) Schematic of the inkjet process and the printed microelectrode arrays.

containing thioether that is suitable for DIW technology was demonstrated.[179] The hydrogel precursor is loaded into a syringe and extruded through a needle. After extrusion, it is rapidly solidified under a 365 nm LED light source. This hydrogel is capable of supporting 3D bioprinting of multiple types of cells, allowing printing at lower concentrations (2 wt%) with high cell survival rates (>80%) and the creation of stable three-dimensional structures (Fig. 10(c)). Similarly, Zhao and coworkers used extrusion-based printing to obtain a ROS-responsive hydrogel scaffold containing a phenylborate structure, which was used to load extracellular vesicles to promote bone healing.[180]

3.3. Inkjet-based fabrication technology

During the inkjet process, ink droplets are ejected from the nozzle and adhered to the surface of the substrate. Thermal and piezoelectric inkjet printings are the two most commonly used drop-on-demand inkjet printing processes (Fig. 9(c)).[181] For thermal inkjet printing, ink is vaporized using a microheater to create a pulse that expels droplets from the nozzle. In piezoelectric inkjet printing, a direct mechanical pulse replacing heating is applied to the ink in the nozzle using a piezoelectric actuator, which causes a shock wave that forces the droplets through the nozzle. Although a hydrogel with shear thinning ability can be printed as ink, the rheological properties of the hydrogel make the deposition process more complicated. Nonetheless, there are still some reports on the construction of organs by inkjet printing.[182–184] Cirelli *et al.* successfully synthesized a new redox-responsive polymer with a PFS skeleton and 5 mol% side groups, which was used as ink to modify the gold surface through inkjet printing.[185] The prepared PSF was dissolved in toluene to obtain oxidation-responsive ink, which was printed using a commercial inkjet printer (nozzle diameter 23 μm and standard droplet 10 pL). AFM shows that the ink droplets can obtain a flat and uniform pattern on the gold substrate. The resulting device was tested using cyclic voltammetry and amperometric measurements, which showed that the device had a sensitive response and stability to ascorbic acid, indicating its potential to be used as an electrochemical sensor array (Fig. 10(d)). Similarly, Kainz *et al.* developed a thiol–yne-based ink. The ink can be quickly cured by UV irradiation after printing and can be integrated into industrial inkjet nozzles. The low biological toxicity of the raw materials makes this ink promising for the development of biological scaffolds.[186]

3.4. Constructing ROS-responsive hydrogel using AM technology

As presented above, laser-, extrusion- and inkjet-based fabrication technologies are mainstream AM technologies, each with its distinct application area. This section will briefly compare these AM technologies from three aspects (fabrication speed, resolution, and substrate range) and focus on the feasibility of constructing ROS-responsive hydrogels. Table 2 gives an overview and comparison with laser-, extrusion- and inkjet-based AM technology.

Table 2 Comparison of standard AM technologies for hydrogel construction

	Laser-based				
Category	SLA	2PP	LIFT	Extrusion-based	Inkjet-based
Resolution (μm)	25–100	0.1	20–100	>100	>50
Fabrication speed	+++	–	++	++	++
Substrate range	+	–	+	+++	++

Generally, fabrication speed and resolution are closely correlated, and the printing speed of laser-based AM technology is the slowest among the three. SLA is the first commercialized AM technology that balances accuracy and speed well. The resolution of products printed by SLA can reach 30 μm by controlling the laser spot size, pulse frequency, and resin layer thickness during fabrication.[187,188] In contrast, 2PP technology, directly engraving model inside the resin which avoids interference from external factors, has the highest manufacturing precision.[189] Up to now, the printing precision of 2PP technology has been able to reach 140 nm (axial) and 90 nm (lateral).[190] However, the high fabrication precision makes the fabrication speed of 2PP drop significantly, which increases its cost and restrains its large-scale application. Therefore, some assistive technologies have been developed to improve the fabrication speed of 2PP. For instance, an ultrafast random-access digital micromirror device (DMD) scanner was developed by Geng and coworkers.[191] By exploiting binary holography, the DMD scanner can simultaneously generate and individually control one to tens of laser foci for parallel nanofabrication at 22.7 kHz (Fig. 11(a)). The total fabrication time of a 10-layer woodpile structure ($36 \times 36 \times 20$ μm^3) *via* three-focus writing mode is 3.6 s. Even so, the writing speed of 2PP is still several orders of magnitude slower than SLA's. For instance, continuous liquid interface production (CLIP) technology was developed by Tumbleston *et al.* based on bottom-up SLA technology,[192] specifically by introducing a reoxygenation thin layer (dead zone) at the bottom of the vat to limit the area where the polymerization occurs, which prevents contact between the hardened resin and the bottom (Fig. 11(b)). Therefore, the link between vibrating and stripping the polymer from the bottom is omitted. CLIP technology shows satisfactory writing speed and accuracy. Furthermore, Lipkowitz *et al.* developed the injection continuous liquid interface production (iCLIP) technology based on CLIP, accelerating printing speeds to 5- to 10-fold over CLIP while maintaining a similar resolution.[193]

SLA and 2PP are laser-based AM technologies, requiring the resin to have polymerizable groups and certain fluidity. As mentioned above, phenylboronic acid-containing hydrogels can be obtained by polymerizing monomers with phenylboronic acid, which fits well with SLA and 2PP technology. For instance, Robinson and coworkers fabricated a dynamic polymer network containing phenylboronate cross-linking units by digital light processing (DLP).[46] The relaxation degree of the printed components could be regulated by adjusting the molar ratio of DABo, DAP, and PETMP. Moreover, when the molar ratio of DABo was equal to 30 mol%, it was difficult for the

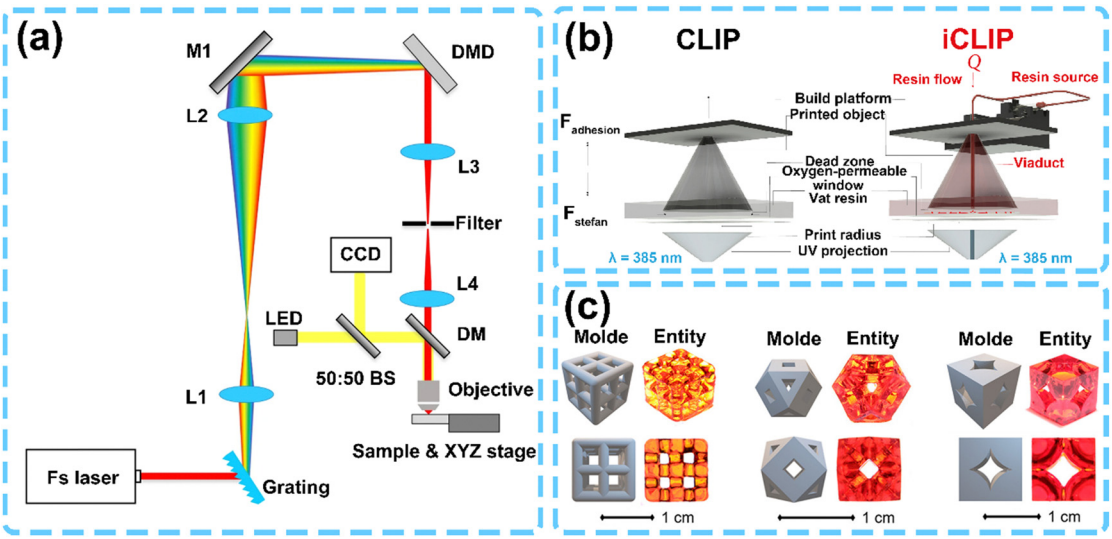

Fig. 11 (a) Optical configuration of the TPP fabrication system. (b) Comparison of CLIP and iCLIP. (c) 3D models of three different lattices and printed products. Reproduced with permission.[26] Copyright 2021, American Chemical Society.

printed object to maintain its original shape, which even showed a certain fluidity. Further research found that the critical proportion of DABo was 25 mol%, which displayed satisfactory printing performance during the subsequent fabrication process. Although it has been reported that the double bond was introduced after the polymer was modified with phenylboronic acid on the side chain, the introduction of phenylboronic acid significantly increased the viscosity of the entire system.[47]

The construction of a Fc-containing ROS-responsive hydrogel leveraging on these two laser-based AM technologies is still inconclusive, and it must be mentioned that due to the unique electrochemical properties and absorption wavelength range (in the visible spectrum) of Fc, many Fc-based photoinitiators have been developed.[194–196] However, this polymerization with Fc and its derivatives as a photoinitiator has specific requirements on the structure of Fc,[197] the design of monomers,[195] and the purity of the solvent.[196] Hence, if SLA or 2PP is employed to fabricate Fc-containing hydrogels, whether and how these factors affect the manufacturing process has to be considered. Nonetheless, it has been reported that the formation of inclusion complexes could improve the stability of guest molecules.[198–200] Taking β-cyclodextrin (β-CD) as an example, when Fc-cyclodextrin inclusion complexes were formed, the absorption peak of Fc around 450 nm disappeared obviously.[195,201] While this phenomenon did not offer conclusive evidence for the SLA and 2PP printability of Fc-containing hydrogels, it did provide a suggestive indication. Moreover, hydrogels containing thioacetal/thioketal and thioethers could theoretically be fabricated using SLA technology *via* thiol–ene (Click) reactions.[202,203] However, as for diselenide bond-containing hydrogels, the diselenide bonds will be broken and rebuilt under ultraviolet irradiation,[138] and this random process will introduce uncertainty into the manufacturing process. Therefore, diselenide bond-containing hydrogels are not suitable for SLA technology.

Distinct from other AM technologies, DIW is not limited by materials. As long as the precursor ink displays appropriate rheological behavior, such as apparent viscosity and shear thinning, it can be utilized for DIW.[204,205] Therefore, the ink for DIW can be freely customized under the condition that the prerequisite. Specifically, a DIW ink should have a yield stress above which the ink will flow. From this, yield stress follows a high viscosity at low rates and enables the ink to maintain a paste-like consistency. Moreover, shear-thinning behavior permits the ink to be extruded, and thixotropy contributes to recovery of the high viscosity after extrusion. The printing accuracy of DIW is mainly affected by the nozzle size and printing speed. Generally, a nozzle with a smaller diameter can improve printing resolution, but it will also require more significant pressure and longer printing time to avoid nozzle clogging. Additionally, the rheological properties of the ink will also significantly impact the resolution of the product. This primarily manifests in two aspects: the extrusion process runs smoothly without blockage, and the ink maintains model structure fidelity during deposition. Therefore, once smoothly discharged from the nozzle, the ink must rapidly transition from the shear-thinning fluid to a solid-like substance to maintain the shape fidelity of the printed product. Typically, the viscosity of the DIW ink falls between the 10^2 and 10^6 mPa s range at a shear rate of approximately 0.1 s^{-1} to ensure the printability of the ink.[206] In the work of Feng and coworkers, an ink was prepared by cross-linking hyaluronic acid modified with methacrylate and phenylboronic acid groups (HAMA–PBA) and methacrylated gelatin (GelMA) for print *via* DIW.[207] This ink exhibited a lower viscosity (10^3 Pa s) at a shear rate of approximately 0.1 s^{-1}, while at rest, the viscosity increased significantly to reach 56 210 Pa s, which exhibited excellent printing performance. Furthermore, as a multi-component printing technology, DIW could achieve gelation during extrusion by blending two or more solutions. For instance, in the

work of Mohand and colleagues, gel filaments with a diameter of approximately 0.3 mm were obtained by irradiating a mixture of a double bond-containing monomer and a thiol-containing monomer with ultraviolet rays immediately after extrusion from a nozzle.[208]

Although both LIFT and inkjet printing are non-contact printing technologies, there are still many differences between them. LIFT is unsuitable for hydrogel diorama fabrication, and the fabrication *via* inkjet print needs some preconditions. Microdropletization is one of the essential features of inkjet printing. Whether thermal or piezoelectric, it provides pressure in a non-contact manner so that the ink is atomized through the nozzle to form droplets for printing. By adjusting parameters such as the nozzle diameter and pressure, 30–60 μm droplets can be produced with a volume of less than 10 pL.[209] The diameter and profile of the incident laser beam control the shape and size of the transferred ink in LIFT. In the work of Visser *et al.*, a copper pillar with a diameter of 5 μm and a height of 2 mm was prepared by LIFT technology.[210] In this process, the metal melts to form droplets, drips, and deposits and forms the model with the irradiation of laser pulses. If a hydrogel is used as the printing material, it is crucial to consider whether its viscosity is sufficient to support the formation of stable three-dimensional structures and whether its toughness is enough to resist the shock of the transfer process (in existing reports, the velocity of droplets during transfer can reach 460 m s^{-1}).[211] Although there have been some reports on bioprinting using LIFT technology, the resulting product in these reports has more of a two-dimensional pattern rather than an actual three-dimensional model.[212–214]

Inkjet printing is similar to DIW in that not limited by materials, and only the rheological properties of the ink are required. Since inkjet print requires the ink to be atomized to form droplets, the viscosity of the ink is usually needed to be 3.5–12 mPa s.[215] However, with the development of electrostatic inkjet printing technology, the critical viscosity of the ink can reach 2000 mPa s.[216] In general, inkjet printing still requires ink with viscosity in the range of 3–30 mPa s, a surface tension of 20–70 mJ m^{-2}, and a density of $\sim$1000 kg m^{-3}.[217] Direct inkjet printing from hydrogels is prone to causing blockages. It is suggested that the gelation of hydrogels could be achieved synchronously during the printing process by evaporation, environmental changes, or chemical cross-linking agents.[181] For example, by virtue of the interaction between alginate and calcium ions, calcium chloride solution could be printed on the alginate solution's surface *via* inkjet printing to prepare an alginate hydrogel scaffold.[218,219] Although there are few reports on the fabrication of ROS-responsive hydrogels by inkjet printing, in principle, the combination of 1,4-phenylenebisboronic acid and polysaccharides has a high similarity to the combination of alginate and calcium ions.

Furthermore, it remains a pressing issue to establish the connection between specific ROS response modules and the mechanical properties of hydrogels for evaluating their printability. Some literature reports indicate that the mechanical properties of ROS-responsive hydrogels are not primarily dependent on the content of ROS-responsive modules.[66,220,221] However, certain papers suggest that the content of these modules can significantly impact the rheological properties of hydrogels.[222,223] Moreover, due to the intricate nature of ROS response processes, their dynamics and reactivity also intricately influence the mechanical properties of hydrogels.[224,225] Given the current dearth in research regarding the precise relationship between the ROS response modules and the hydrogel printing performance, it is challenging to discuss this matter solely from a theoretical standpoint. As mentioned earlier, existing studies have indicated a correlation between the hydrogel printing performance and the viscosity. It is anticipated that in future endeavors, a direct association between the ROS response modules and mechanical properties can be further elucidated.

4. Biomedical applications of ROS-responsive hydrogels

4.1. Dressings

According to the period required for wound healing, wounds can be divided into acute and chronic.[226] Although most acute wounds can be smoothly restored with appropriate treatment, some acute wounds deteriorate into chronic wounds under diabetes,[227] bacterial infection,[228,229] *etc.* Even though some hydrogel wound dressings have been developed and applied to clinics, there are still some requirements that current hydrogel wound dressings can not meet. For instance, chronic wounds are generally accompanied by inflammatory and abnormal ROS levels, both of which inhibit wound healing and significantly burden patients.[230,231] Currently available hydrogel wound dressings lack the ability to adapt to changing wound conditions. However, ROS-responsive hydrogels have the unique capability to adjust their properties in real-time during the wound-healing process. Their responsiveness to abnormal levels of ROS produced as a result of inflammation makes them the superior choice for wound care. Wang *et al.* developed a ROS-responsive shape-adaptable hydrogel (DPE) based on phenylboronate with antibacterial properties (Fig. 12(a)).[232] This hydrogel was synthesized through stepwise addition of DL-dithiothreitol, poly(ethylene glycol)diacrylate, and phenylboronic acid-modified ε-polylysine, and generated *in situ* under partial irradiation. DHE showed a sensitive response to ROS and a strong ROS elimination ability. When incubated with H_2O_2, it was able to eliminate over 50% of H_2O_2. Additionally, DPE hydrogels exhibited significant cytocompatibility and powerful antibacterial properties, specially more than 99% of *E. coli*, *S. aureus*, and MRSA on the surface of DPE2 were killed. Furthermore, a full-thickness skin defect model infected by *S. aureus* was established on SD rats to assess the efficacy of DPE hydrogels in promoting wound healing compared with the control of standard gauze. Wounds treated with DPE2 exhibited a smaller wound area and superior healing compared to the other treatments at the same time point. After 14 days, the reconstruction of epithelial and dermal structures was

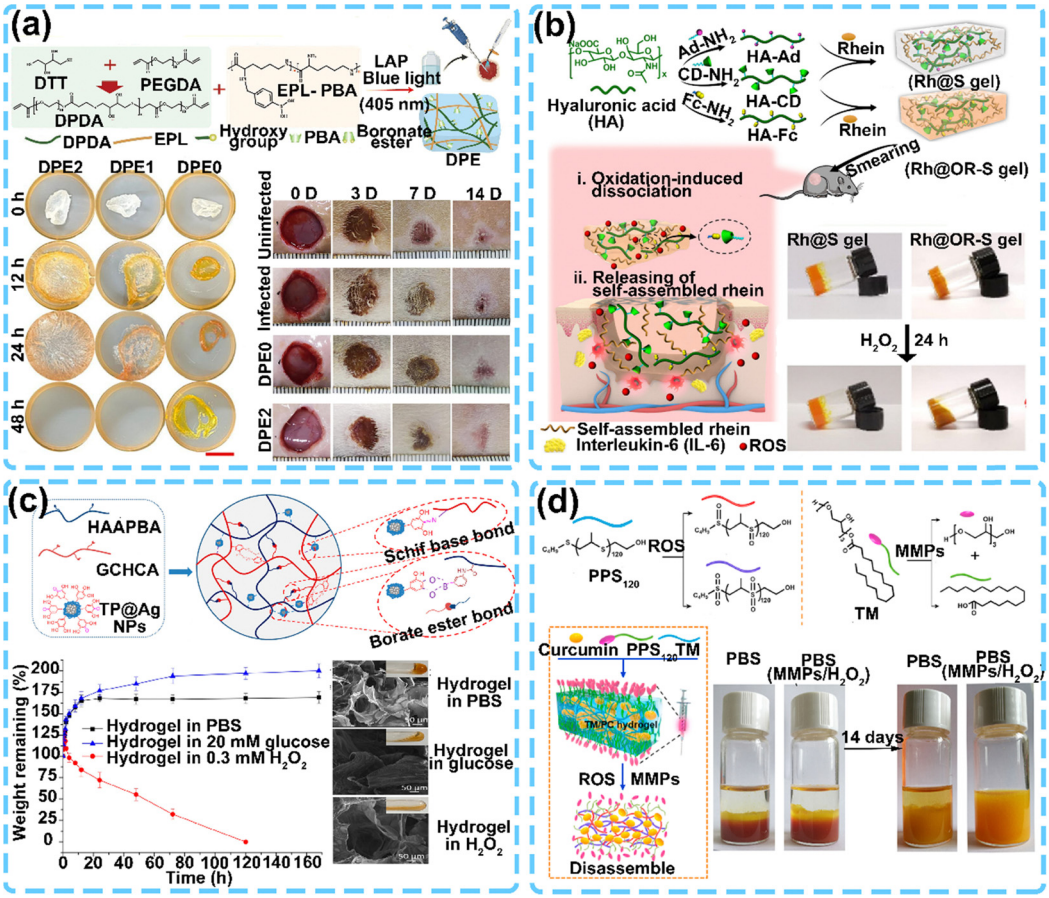

Fig. 12 (a) DPE hydrogel preparation and images of wounds treated with various samples at different times. Reproduced with permission.[154] Copyright 2022, Elsevier. (b) Synthetic route of the oxidation-responsive supramolecular hydrogel and the treatment of wound. Reproduced with permission.[155] Copyright 2020, American Chemical Society. (c) The preparation of glucose/ROS-sensitive network and its ROS-responsive ability. Reproduced with permission.[19] Copyright 2023, American Chemical Society. (d) Formation and mechanism of the TM/PC hydrogel in TBI. Reproduced with permission.[64] Copyright 2021, Elsevier.

satisfactory in all treatment groups. Analogously, Zhao and colleagues reported a supramolecular hydrogel dressing based on the interaction between Fc and β-CD (Fig. 12(b)).[233] Two new polymers, HA-Fc and HA-CD, were created by modifying the HA backbone with Fc and β-CD, respectively. A ROS-responsive hydrogel, Rh@OR-S gel with rhein, was then rapidly prepared through one-pot mixing. Meanwhile, the Rh@S gel lacking ROS-responsiveness was designed through the same process but replacing Fc with adamantane. The Rh@S gel could maintain its solid state in normal and oxidative environments. In contrast, the Rh@OR-S gel exhibited similar stability to the Rh@S gel under normal conditions but displayed noticeable mobility under oxidative conditions. Furthermore, a diabetic C57 mouse model was first established using streptozocin (STZ). By measuring the percentage of the reduced wound area, the wounds treated with the Rh@OR-S gel healed faster than others, and the wound closure ratio of which was significantly higher. Among all the groups, the Rh@OR-S gel demonstrated the most efficient pro-wound healing efficacy, nearly complete epithelial coverage, and an epidermal thickness closely resembling healthy skin. Furthermore, in the work of Zhou *et al.*, introducing a mussel-like super-adhesive with catechol groups and glucose/ROS-sensitive dynamic phenylborate cross-linking network allows for *in situ* construction of hydrogels in just 21 seconds (Fig. 12(c)).[38] This hydrogel offers excellent injectability, self-healing, tissue adhesion, and glucose/ROS-sensitive drug release properties. The hydrogel can be fully injected and adhered to irregular wound tissue, and its swelling ratio of about 150% allows it to reduce physical pressure on the wound surface, absorb liquid exuded from the tissue, and maintain a moist environment. The hydrogel's ROS scavenging ability and regulation of macrophage M2 polarization can reduce the inflammatory response and significantly promote infected diabetic wound healing.

Traumatic brain injury (TBI) is an injury to the brain caused by an external force. Open wounds and ROS overproduction are characteristic features of TBI and tend to cause serious secondary injury. The using of ROS-responsive hydrogels is a promising therapeutic strategy to protect wounds and control ROS levels. In the work of Qian *et al.*, an injectable ROS-responsive hydrogel-embedded curcumin (Cur) (TM/PC) was developed to promote the regeneration of neurons after TBI (Fig. 12(d)).[64] The hydrogel composed matrix metalloproteinase (MMP)-

responsive triglycerol monostearate (TM) and ROS-responsive hydrophobic poly(propylene sulfide)$_{120}$ (PPS_{120}). It was found that the using of the TM/PC hydrogel effectively reduced the level of ROS in the brain injury site of TBI mice, and avoided the occurrence of brain edema. Moreover, after hydrogel treatment, the blood–brain barrier (BBB) permeability of TBI mice and penetrating brain injury (PBI) significantly decreased, showing good recovery. Notably, doublecortin (DCX) is a microtubule-associated protein expressed by neuronal precursor cells and immature neurons,[234] and there was a significant increase of DCX after TM/PC hydrogel treatment, suggesting neurological repair in progress.

4.2. Drug delivery

Drug carriers aim to increase drug concentration at the site of the lesion, reducing exposure in normal tissue and minimizing side effects, ultimately alleviating patient discomfort.[235] Nanoparticles are a common strategy for encapsulating and delivering drugs to target tissue without a spill.[236] Although nanoparticles have great modifiability, which allows an efficient encapsulation of almost all drugs, some nanoparticles will inevitably be retained in filtration organs (such as the liver and spleen) or cleared by macrophages in the circulatory system.[237,238] In contrast, hydrogel drug carriers offer significant advantages by minimally invasive drug delivery *in situ* to target tissues and maximum reducing exposure in normal tissues. Although conventional hydrogels can deliver drugs *in situ*, the release process is typically prolonged and gradual (ranging from hours to days, weeks, or even months, depending on the formulation).[9] The sustained release of drugs is advantageous for chronic diseases, such as diabetes, but it may have little effect during the acute phase of some illnesses.[239] An abnormal level of ROS is a significant part of severe inflammatory responses, which is a typical feature of most acute diseases. Due to its high sensitivity to ROS, the ROS-responsive hydrogel can self-regulate drug release rates in response to varying degrees of inflammation, especially in the acute phase of the disease, drug release can be selectively enhanced to timely control further disease progression.

Cancer is one of the deadliest diseases of human beings, and has caused a great burden on public health.[240] Injectable hydrogels show great potential for drug delivery without surgical operations and improving cancer therapies.[241] In the study conducted by Dai and colleagues, a new type of hydrogel that is responsive to both pH and ROS was created (Fig. 13(a)).[242] This hydrogel could carry an integrated inorganic sonosensitizer (TiOx@CaO_2) and an immune checkpoint inhibitor (aPD-L1). A TiOx@CaO_2@TSPBA-PVA hydrogel was formed *in situ* rapidly by reacting phenylboronic acid and PVA. After forming, ultrasound could trigger the decomposition of TiOx@CaO_2, which generated ROS. This process reversed the tumor hypoxic microenvironment and destroyed the phenylboronate, resulting in aPD-L1 release. The decomposition of TiOx@CaO_2 also produced a large amount of Ca^{2+}, which worked together with aPD-L1 for treatment. Therefore, TiOx@CaO_2 released approximately 20% in PBS at pH 7.4 within two days but reached up to 50% under acidic and oxidizing conditions. When only treated with TiOx@CaO_2, the tumor inhibition rate was only 36.6%, but after ultrasound assistance, the inhibition rate increased to 62%. After adding aPD-L1 further, the inhibition rate reached 89%. Moreover, in the study of Wang *et al.*, a ROS-responsive hydrogel (GEM-STING@Gel) was engineered to co-deliver gemcitabine and the stimulator of interferon genes (STING) agonist 5,6-dimethylxanthenone-4-acetic acid (DMXAA) (Fig. 13(b)).[243] This hydrogel effectively activates the immune response against pancreatic cancer cells, while halving the dosage and frequency of medication, due to its efficient and precise drug delivery system, significantly enhancing drug bioavailability. In summary, ROS-responsive hydrogels have been employed in cancer therapy research, and significant advancements have been achieved in laboratory settings.

Myocardial infarction (MI) is one of the leading causes of mortality worldwide.[244] Injectable hydrogels are ideal materials for the efficient treatment of MI owing to the direct injection into the infarcted area and mechanical support to the ventricular wall, which inhibits negative remodeling of the left ventricle.[245] Restoring intracellular redox homeostasis is important to prevent further myocardial infarction caused by ROS produced due to mitochondrial dysfunction. In the study of Li and colleagues, a ROS-responsive phenylboronate-containing hydrogel was prepared to deliver basic fibroblast growth factor (bFGF) for MI treatment by injection into the pericardial cavity (Fig. 13(c)).[246] In the normal environment simulated *in vitro*, bFGF showed slow release, but with the introduction of H_2O_2 (0.5×10^{-3} mM), the release rate increased significantly. Co-incubating the hydrogel and neonatal rat cardiomyocytes (NRCMs) with H_2O_2 increases NRCM proliferation due to increased bFGF release compared to the hydrogel without H_2O_2. After injecting the hydrogel into MI model rats, the number of Ki67-positive cells significantly increased in the peri-infarct region, indicating that the hydrogel promoted endogenous cell proliferation. Additionally, there are a decrease in the scar size and an increase in the viability of the myocardium, suggesting a good recovery in the peri-infarct region. Similarly, Zhang and colleagues designed a novel drug delivery system using a mitochondria-targeted Szeto-Schiller (SS31) peptide-modified amphiphilic polymer (PTPS) to encapsulate cyclosporine A (CsA). The CsA-loaded nanomicelles (PTPSCs) were then incorporated into an injectable hydrogel that is responsive to both pH and ROS through reversible imine and phenylboronate interactions (Fig. 13(d)).[41] Under the oxidizing conditions present in the infarct region, the phenylboronate underwent degradation, leading to the release of PTPSCs. Then PTPSCs released CsA in the process of scavenging ROS and inhibited the mitochondria-mediated apoptosis signaling pathway to prevent myocardial apoptosis. After the treatment, the echocardiography of I/R rats showed significant ventricular wall motion disturbance as compared to the sham operation group. This indicates persistent myocardial damage caused by MI. However, rats treated with the hydrogel showed similar echocardiography results to the rats in the sham operation group. Furthermore, the ventricular wall thickness returned to

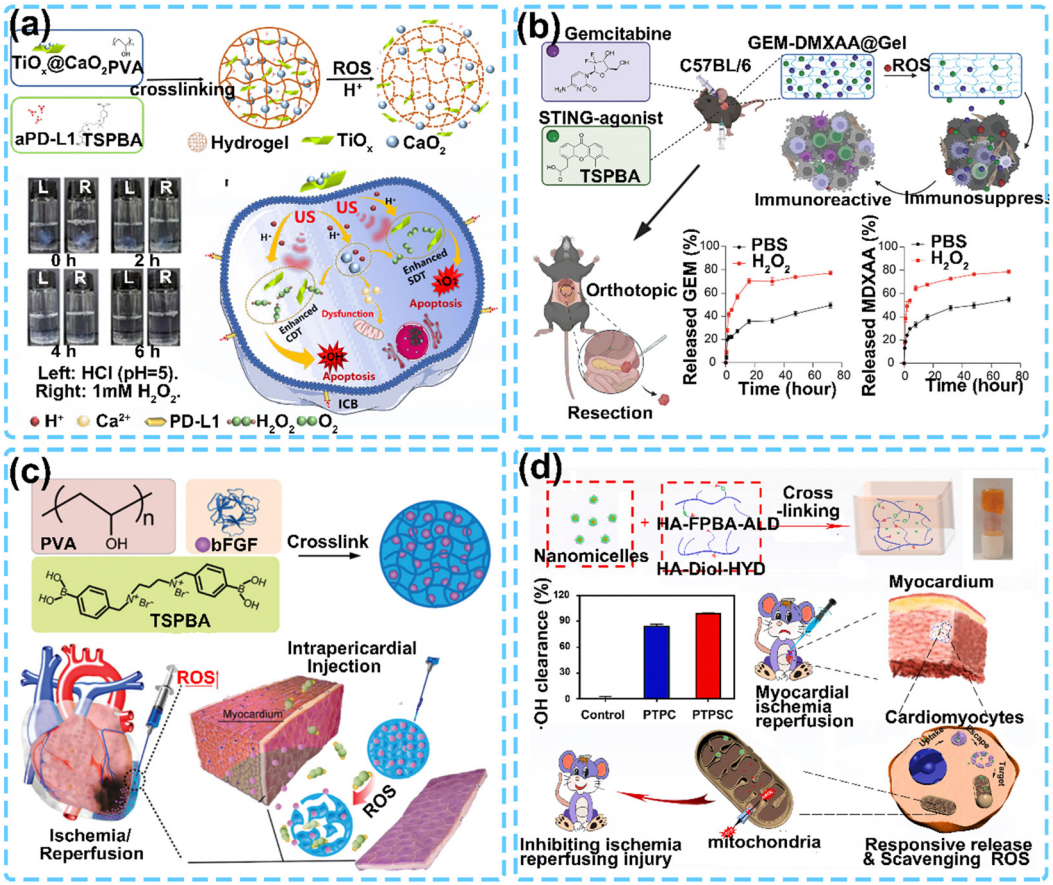

Fig. 13 (a) Schematic representation of the construction of a dual-responsive niche-like hydrogel and its therapeutic mechanism. Reproduced with permission.[163] Copyright 2023, Elsevier. (b) Illustration of immunotherapy strategy using a ROS-responsive hydrogel to deliver gemcitabine and STING agonist into the pancreatic tumor for immune regulations. Reproduced with permission.[164] Copyright 2023, Wiley-VCH. (c) Schematic illustration of Gel-bFGF fabrication and overall strategy. Reproduced with permission.[165] Copyright 2021, Wiley-VCH. (d) The preparation of PTPSCs and its treatment mechanism for MI. Reproduced with permission.[41] Copyright 2022, Elsevier.

normal levels after hydrogel treatment, demonstrating good therapeutic efficacy for acute MI.

4.3. Cellular therapy

To live, proliferate, and migrate, many cells require an extracellular matrix to play the role of structural support and anchorage.[9] Once detached from the extracellular matrix, most cells undergo a specific type of programmed cell death known as anoikis.[247] This poses a significant challenge to cellular therapy because free cells are difficult to maintain viablity in target tissues and are easily cleared by immune cells. Moreover, given that many diseases are accompanied by inflammation, the overproduction of ROS could cause severe damage to cellular viability. Therefore, using ROS-responsive hydrogels for constructing cell scaffolds is undeniably appealing for providing valuable 3D templates for tissue regeneration and adoptive cell therapy. Stem cell-based therapy is an important branch of regenerative medicine to enhance the body repair machinery *via* stimulation, modulation, and regulation of the endogenous stem cell population and replenishing the cell pool toward tissue homeostasis and regeneration.[248–250] This process has to use carriers to ensure that the activity of stem cells is well-maintained. In the work of Martin and colleagues, a ROS-responsive stem cell delivery platform with powerful cytocompatibility was prepared (Fig. 14(a)).[55] It was observed that cell infiltration and material remodeling were more prominent in PTK hydrogel implants compared to PEG-dt implants (without ROS-responsiveness), demonstrating excellent biocompatibility. A spinal cord injury (SCI) can be a devastating disabling event that often leads to severe dysfunction of the limbs below the injured segment of the spinal cord.[251] The injury process is accompanied by complex inflammation-related pathological processes and apoptosis of various neurons, including neuronal cells, glial cells, and oligodendrocytes. These factors make treating SCI a significant challenge. In the study of Li and colleagues, a ROS-responsive hydrogel (THIEF) based on thioketal was prepared for encapsulation of the bone marrow-derived mesenchymal stem cells (BMSCs) to reconstruct the SCI microenvironment and promote injury nervous system regeneration (Fig. 14(b)).[56] The hydrogels that encapsulated BMSCs demonstrated a powerful anti-inflammatory capacity. During the *in vitro* inflammation

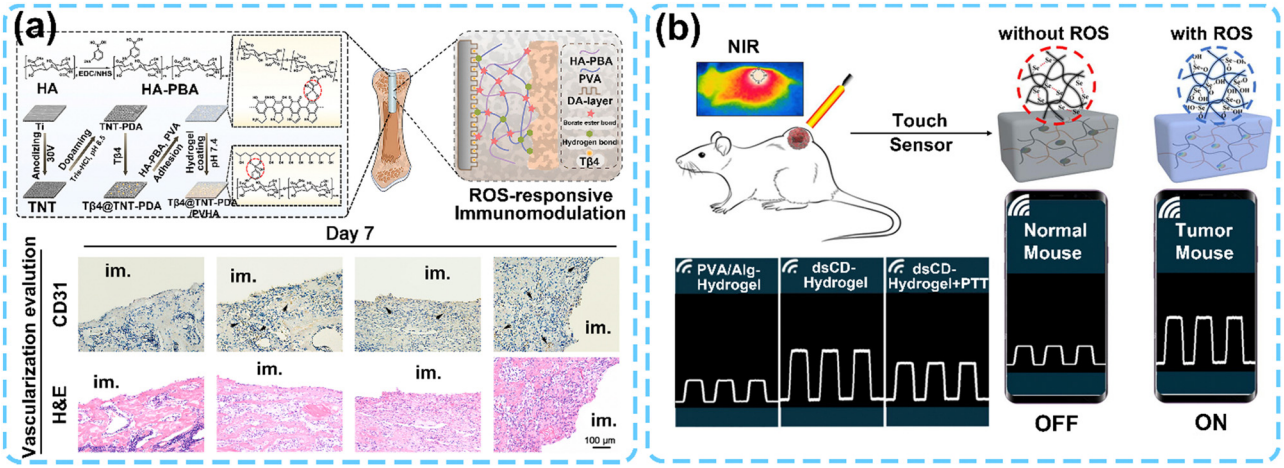

Fig. 14 (a) Synthesis schemes for the PEG–MAL–PTK macromer and its ROS-responsive ability. Reproduced with permission.[38] Copyright 2020, Elsevier. (b) Schematic illustration of the BMSC-encapsulated ROS-scavenging hydrogel for spinal cord injury treatment.

simulation, the viable cell count was 65.6 ± 4.0% in the THIEF group, which was similar to that of normal conditions (70%). Additionally, when the THIEF hydrogel was implanted into the spinal cord injury gaps of rats, the $^{\bullet}O^{2-}$ level in the spinal cord injury site significantly reduced for 7 days. Simultaneously, the marker for oxidative damage to DNA, 8-hydroxy-2′-deoxyguanosine (8-OHdG), decreased from 29.1 ± 7.2 in the model group to 16.7 ± 4.8, suggesting significant suppression of DNA damage through ROS scavenging. Similarly, ROS-responsive hydrogels are also used to deliver probiotics. In the work of Huang and colleagues, a ROS-responsive hydrogel based on the crosslinking of methacrylate-modified hyaluronic acid (MeHA) and thiolated thioketal was prepared to protect and precisely deliver probiotics for inflammatory bowel disease (IBD).[58] By adding Lactobacillus reuteri (LR) to the precursor solution of the hydrogel to encapsulate it, the encapsulation rate could reach 95% and the survival rate was 90%. In contrast, the survival rate of free probiotics was only approximately 60%. This hydrogel exhibited strong retention in the intestine, and HA-LR hydrogel treatment resulted in preservation of the colon length in colitis mice, which was similar to that of the normal mice. Additionally, these epithelial damage and inflammation were largely attenuated by HA-LR treatment with significantly decreased levels of TNF-α and IL-6, both of which were representative pro-inflammatory cytokines.

4.4. Other applications

Hydrogels that respond to ROS can serve as a surface coating for medical implants to modify their properties. This coating can enhance the compatibility of the implants with the human body, particularly for long-term implants like orthopedic ones, by promoting adhesion and preventing inflammation. For instance, Li *et al.* developed a ROS-responsive hydrogel loaded with thymosin β4 (Tβ4) for surface modification of titanium-based implants (Fig. 15(a)).[252] This coating, based on polyvinyl alcohol (PVA) and phenylboronic acid-modified hyaluronic acid (HA-PBA), demonstrated remarkable anti-inflammatory properties and enhanced bone regeneration capabilities *in vivo*. Specifically,

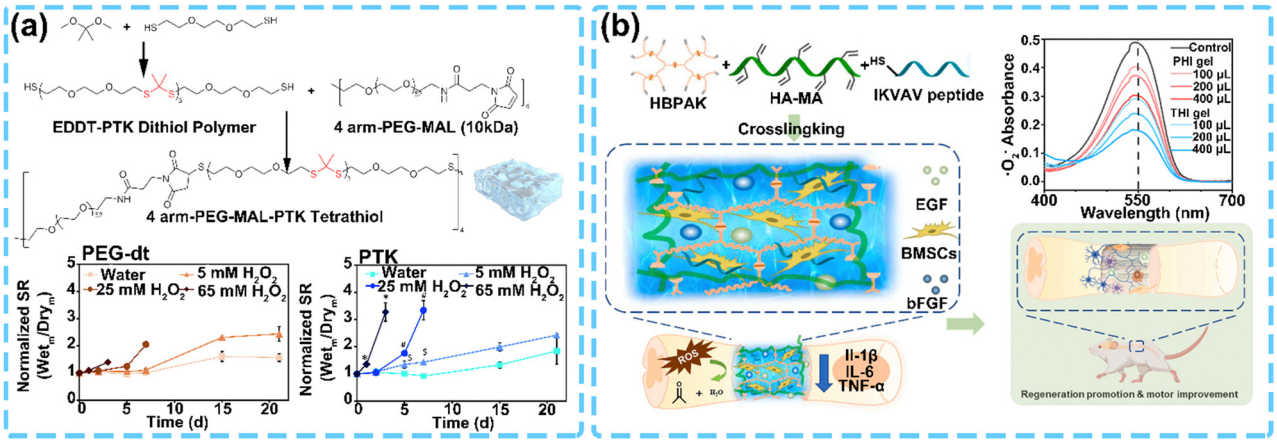

Fig. 15 (a) Schematic representation of preparing hydrogel-coated implants and their promotion of *in vivo* blood vessel growth. Key: im., implants. Reproduced with permission.[21] Copyright 2022, Elsevier. (b) Schematic showing how the hydrogel sensor works and an example of pressure sensing *in vivo*. Reproduced with permission.[71] Copyright 2023, Elsevier.

with the treatment using a hydrogel-modified implant (Tβ4@TNT-PDA/PVHA), the number of M2 phenotype macrophages ($CD206^+$) at the implant site significantly increased, which further resulted in more pronounced cell growth. Meanwhile, the histological analysis of vascularization reflected the formation of a more mature vascular network adjacent to Tβ4@TNT-PDA/PVHA compared to other implants, which is a typical prerequisite for bone repair. Moreover, ROS-responsive hydrogels could also be employed in applications such as hydrogel sensors. With the advent of the information age, people seek real-time monitoring of analytes in the body for personalized healthcare. The demand for materials that facilitate the integration of implantable sensors with the human body is also on the rise. Hydrogel, being a potential option for developing implantable sensors, has been widely studied for constructing such sensors. In the work of Jo and coworkers, a wireless pressure sensor based on the ROS responsiveness of the diselenide bond was designed for the selective detection of the tumor microenvironment (Fig. 15(b)).[71] In the environment surrounding a tumor, the diselenide bond of the hydrogel was broken down by ROS, which strengthened the hydrogen bond force within the hydrogel. As a result, the hydrogel showed an increase of 52% in electrical conductivity, 122% in mechanical tensile properties, and 91% in the strain–pressure response. Additionally, this effect could be detected through wireless sensor devices, which further could be accessed on a smartphone.

5. Conclusions and perspectives

ROS-responsive hydrogels have gained attention in the biomedical field due to their unique properties, although they have a relatively short history of development. However, the intricate behavioral characteristics of ROS pose significant challenges to certain the detailed degradation process of ROS-responsive materials. Moreover, the structure of a hydrogel will directly affect the response speed and degradation efficiency of the hydrogel. For example, a dense surface layer will form on the surface of hydrogels obtained by free radical polymerization, which limits the diffusion of water molecules and other molecules, which reduces the sensitivity of the response.[253] In addition, in the hydrogel structure synthesized by cross-linking agents and monomers, hydrogels with a highly heterogeneous structure will be formed due to the difference in reactivity of the monomers and cross-linking agents. During network formation, dense clusters are formed in the early stages of chain growth aggregation and are connected by bridge aggregation chains in subsequent stages. However, after cluster formation, the polymerization solution becomes more viscous, resulting in an asymmetric distribution of clusters in the hydrogel.[254] There are currently two strategies for optimizing the structure of stimulus-responsive hydrogels. One is to increase the specific surface area of the hydrogel to enhance the response sensitivity by constructing a porous structure or a comb structure.[255,256] The second is to improve the response dynamics of responsive hydrogels by incorporating nanocomposite structures similar to microspheres or micelles into the hydrogel structure.[257] But there is still a long way to go before we can completely solve this problem and establish a direct relationship between the hydrogel structure and responsiveness. Therefore, considering factors such as safety, strength, versatility, and cost, the clinical application of these hydrogels still has many challenges. Additionally, another important challenge for chemical and scientific researchers is to pattern the surface of ROS-responsive hydrogels through AM technologies to adjust their response time and intensity to meet different requirements. Not only that, the better combinations of AM technologies and ROS-responsive hydrogels are also a problem that needs to be solved urgently. Currently, the research and development of ROS-responsive hydrogels rely mostly on experimental testing methods. The process of creating a hydrogel with ideal properties in terms of mechanical strength, tissue adaptation, and responsive degradation often requires a lot of attempts. With the advancement of computers, computer-assisted simulation analysis has made impressive achievements in small molecule synthesis through synthetic route design, reaction site prediction, and impurity analysis. The mechanical strength and thermal behavior of hydrogels are determined by their atomistic description. Atomistic level simulations are the most appropriate approach to capture the deformation governing mechanism. Although numerical simulation techniques such as first principles calculations, *ab initio* methods, density functional theory, and quantum-based practices are highly precise and comparable to experimental techniques, they have a limitation regarding the number of atoms they can handle in a simulation. Generally, they can only handle a few thousand atoms in a simulation, which means they are appropriate for simulating small molecules, but not suitable for larger structures like hydrogels. Among these simulations, the molecular dynamics (MD)-based approach is emerging as a promising technique for simulating the mechanical and thermal behavior of hydrogels. This simulation method is based on the principles of Newtonian mechanics and can determine the trajectory of particles in the system. Although it ignores some special circumstances of atoms or molecules under quantum mechanics, it can numerically analyze the Newtonian equations of motion of interacting particles for more complex and large systems. The force and potential energy between particles are determined using the molecular mechanics force field. For instance, in 2018, Kanduc *et al.*[258] elucidated the diffusion behavior of polar and nonpolar penetrants in thermal-responsive PNIPAM hydrogels using MD-based simulations. The PNIPAM was modeled using an OPLS-based force field. It may soon be possible to use computers to design and optimize hydrogel structures, leading to quicker production of high-performance ROS-responsive hydrogels in labs. Additionally, it is also critical to strengthen the connection between ROS-responsive hydrogels and AM technologies. As analyzed previously, for ROS-responsive hydrogels, extrusion-based AM technology has extremely high universality, but is limited by the processing accuracy and the viscosity of ink. The hydrogel model obtained by this method has low

resolution and cannot be suitable for some precise occasions. Laser-based AM technology has a certain selectivity for ROS-responsive modules, which cannot process ROS-responsive hydrogels containing ferrocene or diselenide bonds. There is an urgent need for a universal method for industrialized processing and production of ROS-responsive hydrogels to further advance their implementation.

Moreover, finding a way to choose the appropriate ROS response module in the ROS response hydrogel for specific applications is essential. Diseases can be categorized into two types: acute and chronic. ROS response modules are divided into ROS-induced bond cleavage (such as phenylborate and thioketal) and ROS-induced solubility switch (thioether and ferrocene). Studies suggest that ROS-induced bond cleavage structures, when added to drug delivery systems, lead to faster drug release and easier degradation of the drug delivery system, while, ROS-induced solubility switch structures result in a slower degradation rate.[259] Although we can make a preliminary judgment that ROS-responsive structures that react to cleavage are more suitable for acute diseases, and those that respond to phase transitions are more suitable for chronic diseases, we must conduct further research to establish a direct relationship between the disease model and the ROS response module. At present, we can only make rough estimates through empirical judgments.

All these issues need to be urgently solved to advance the clinical transformation of this promising material and benefit more people. We believe that soon researchers will obtain a complete theory, discover more types of ROS-responsive hydrogels with better performance, and promote the clinical transformation of this promising material.

Conflicts of interest

The authors declare no conflict of interest.

Acknowledgements

This work was supported by the National Key R&D Program of China (no. 2019YFA0904500), the National Natural Science Foundation of China (52303193), the Natural Science Foundation of Sichuan Province (24NSFSC6375), and the Fundamental Research Funds for Central Universities.

Notes and references

1 M. C. Koetting, J. T. Peters, S. D. Steichen and N. A. Peppas, *Mater. Sci. Eng., R*, 2015, **93**, 1–49.
2 S. Amirthalingam, A. K. Rajendran, Y. G. Moon and N. S. Hwang, *Mater. Horiz.*, 2023, **10**, 3325–3350.
3 Y. Xu, J. Hu, J. Hu, Y. Cheng, X. Chen, Z. Gu and Y. Li, *Prog. Polym. Sci.*, 2023, **146**, 101740.
4 Z. Zhao, Z. Wang, G. Li, Z. Cai, J. Wu, L. Wang, L. Deng, M. Cai and W. Cui, *Adv. Funct. Mater.*, 2021, **31**, 2103339.
5 C. Wang, C. Liu, Q. Wei, L. Yang, P. Yang, Y. Li and Y. Cheng, *Research*, 2020, **2020**, 6563091.
6 Y. Zhao, S. Song, X. Ren, J. Zhang, Q. Lin and Y. Zhao, *Chem. Rev.*, 2022, **122**, 5604–5640.
7 Y. Fu, J. Zhang, Y. Wang, J. Li, J. Bao, X. Xu, C. Zhang, Y. Li, H. Wu and Z. Gu, *Carbohydr. Polym.*, 2021, **257**, 117598.
8 M. Li, H. Wang, J. Hu, J. Hu, S. Zhang, Z. Yang, Y. Li and Y. Cheng, *Chem. Mater.*, 2019, **31**, 7678–7685.
9 S. Correa, A. K. Grosskopf, H. Lopez Hernandez, D. Chan, A. C. Yu, L. M. Stapleton and E. A. Appel, *Chem. Rev.*, 2021, **121**, 11385–11457.
10 L. Guo, T. Wang, Z. Li, S. Wu, Y. Xu, Z. Yang, Y. Li, Z. Gu and X. Jiang, *Chem. Mater.*, 2023, **35**, 5420–5432.
11 H. Zhang, J. Zhang, X. Peng, Z. Li, W. Bai, T. Wang, Z. Gu and Y. Li, *Adv. Sci.*, 2022, **9**, 2203587.
12 Y. Yang, L. Yang, F. Yang, W. Bai, X. Zhang, H. Li, G. Duan, Y. Xu and Y. Li, *Mater. Horiz.*, 2023, **10**, 268–276.
13 J. Wu, X. Wu, F. Yang, X. Liu, F. Meng, Q. Ma and Y. Che, *Int. J. Biol. Macromol.*, 2023, **225**, 1119–1128.
14 S. Tamesue, S. Noguchi, Y. Kimura and T. Endo, *ACS Appl. Mater. Interfaces*, 2018, **10**, 27381–27390.
15 R. P. Brannigan and V. V. Khutoryanskiy, *Macromol. Biosci.*, 2019, **19**, 1900194.
16 L. d'Amone, J. K. Sahoo, N. Ostrovsky-Snider, D. L. Kaplan and F. G. Omenetto, *Biomacromolecules*, 2023, **24**, 1310–1317.
17 B. D'Autréaux and M. B. Toledano, *Nat. Rev. Mol. Cell Biol.*, 2007, **8**, 813–824.
18 B. Yang, Y. Chen and J. Shi, *Chem. Rev.*, 2019, **119**, 4881–4985.
19 P. Yang, Z. Gu, F. Zhu and Y. Li, *CCS Chem.*, 2020, **2**, 128–138.
20 Y. Nosaka and A. Y. Nosaka, *Chem. Rev.*, 2017, **117**, 11302–11336.
21 M. Hayyan, M. A. Hashim and I. M. AlNashef, *Chem. Rev.*, 2016, **116**, 3029–3085.
22 D. R. Kearns, *Chem. Rev.*, 2002, **71**, 395–427.
23 H. Sies and D. P. Jones, *Nat. Rev. Mol. Cell Biol.*, 2020, **21**, 363–383.
24 B. Wu, F. Qi and Y. Liang, *Trends Plant Sci.*, 2023, **28**, 1124–1131.
25 I. S. Harris and G. M. DeNicola, *Trends Cell Biol.*, 2020, **30**, 440–451.
26 G. Wang, F. Yang, W. Zhou, N. Xiao, M. Luo and Z. Tang, *Biomed. Pharmacother.*, 2023, **157**, 114004.
27 T. Lopez, M. Wendremaire, J. Lagarde, O. Duquet, L. Alibert, B. Paquette, C. Garrido and F. Lirussi, *Biomedicines*, 2022, **10**, 2784.
28 H. M. El-Husseiny, E. A. Mady, L. Hamabe, A. Abugomaa, K. Shimada, T. Yoshida, T. Tanaka, A. Yokoi, M. Elbadawy and R. Tanaka, *Mater. Today Bio*, 2022, **13**, 100186.
29 Q. Xu, C. He, K. Ren, C. Xiao and X. Chen, *Adv. Healthcare Mater.*, 2016, **5**, 1979–1990.
30 Y. Chen, W. Wang, D. Wu, H. Zeng, D. G. Hall and R. Narain, *ACS Appl. Mater. Interfaces*, 2019, **11**, 44742–44750.
31 H. Kang, W. Wei, L. Sun, R. Yu, E. Yang, X. Wu and H. Dai, *Chem. Mater.*, 2023, **35**, 2408–2420.

32 M. Zhang, C.-C. Song, F.-S. Du and Z.-C. Li, *ACS Appl. Mater. Interfaces*, 2017, **9**, 25905–25914.
33 S. Wang, Y. Liu, Q. Sun, B. Zeng, C. Liu, L. Gong, H. Wu, L. Chen, M. Jin, J. Guo, Z. Gao and W. Huang, *Adv. Sci.*, 2023, **10**, 2303167.
34 W. Zhang, K. Zha, Y. Xiong, W. Hu, L. Chen, Z. Lin, C. Yu, W. Zhou, F. Cao, H. Hu, B. Mi and G. Liu, *Bioact. Mater.*, 2023, **30**, 29–45.
35 Y. Ma, P. He, W. Xie, Q. Zhang, W. Yin, J. Pan, M. Wang, X. Zhao and G. Pan, *Research*, 2021, **2021**, 9565402.
36 W. Shi, F. Fang, Y. Kong, S. E. Greer, M. Kuss, B. Liu, W. Xue, X. Jiang, P. Lovell, A. M. Mohs, A. T. Dudley, T. Li and B. Duan, *Biofabrication*, 2021, **14**, 014107.
37 W. Shi, B. Hass, M. A. Kuss, H. Zhang, S. Ryu, D. Zhang, T. Li, Y.-L. Li and B. Duan, *Carbohydr. Polym.*, 2020, **233**, 115803.
38 X. Zhou, X. Ning, Y. Chen, H. Chang, D. Lu, D. Pei, Z. Geng, Z. Zeng, C. Guo, J. Huang, S. Yu and H. Guo, *ACS Mater. Lett.*, 2023, **5**, 3142–3155.
39 T. Hao, M. Qian, Y. Zhang, Q. Liu, A. C. Midgley, Y. Liu, Y. Che, J. Hou and Q. Zhao, *Adv. Sci.*, 2022, **9**, 2105408.
40 S. Wang, Y. Yao, T. Zhou, J. Xie, J. Ding, W. Cao, L. Shen, Y. Zhu and C. Gao, *Composites, Part B*, 2022, **238**, 109941.
41 X. Zhang, Y. Sun, R. Yang, B. Liu, Y. Liu, J. Yang and W. Liu, *Biomaterials*, 2022, **287**, 121656.
42 P. Tournier, G. Saint-Pé, N. Lagneau, F. Loll, B. Halgand, A. Tessier, J. Guicheux, C. L. Visage and V. Delplace, *Adv. Sci.*, 2023, **10**, 2300055.
43 A. J. R. Amaral, V. M. Gaspar, P. Lavrador and J. F. Mano, *Biofabrication*, 2021, **13**, 035045.
44 M. Monavari, S. Homaeigohar, R. Medhekar, Q. Nawaz, M. Monavari, K. Zheng and A. R. Boccaccini, *ACS Appl. Mater. Interfaces*, 2023, **15**, 50626–50637.
45 R. P. T. Tan, J. J. W. Cheng, B. H. Parikh, J. H. M. Wong, B. W. Soh, J. J. Chang, K. C. Tran, Y. Lee, P. L. Chee, Y. J. Boo, Q. Lin, L. Jiang, X. Su, J. Y. C. Lim, X. J. Loh and K. Xue, *ACS Appl. Polym. Mater.*, 2022, **4**, 5091–5102.
46 L. L. Robinson, J. L. Self, A. D. Fusi, M. W. Bates, J. Read de Alaniz, C. J. Hawker, C. M. Bates and C. S. Sample, *ACS Macro Lett.*, 2021, **10**, 857–863.
47 H. Gao, C. Yu, Q. Li and X. Cao, *Carbohydr. Polym.*, 2021, **258**, 117663.
48 J. Qin, B. Dong, W. Wang and L. Cao, *J. Colloid Interface Sci.*, 2023, **649**, 344–354.
49 L. Li, J. Xu, J. Li, X. Lyu, Z. Liu and J. Wei, *Sens. Actuators, B*, 2022, **373**, 132721.
50 M. Ni, N. Zhang, W. Xia, X. Wu, C. Yao, X. Liu, X.-Y. Hu, C. Lin and L. Wang, *J. Am. Chem. Soc.*, 2016, **138**, 6643–6649.
51 K. Zhang, X. Feng, C. Ye, M. A. Hempenius and G. J. Vancso, *J. Am. Chem. Soc.*, 2017, **139**, 10029–10035.
52 M. Jain and B. J. Ravoo, *Angew. Chem., Int. Ed.*, 2021, **60**, 21062–21068.
53 S. Mu, W. Liu, L. Zhao, Y. Long and H. Gu, *Polymer*, 2019, **169**, 80–94.
54 L. Folkertsma, K. Zhang, M. A. Hempenius, G. J. Vancso, A. van den Berg and M. Odijk, *Polym. Adv. Technol.*, 2017, **28**, 1194–1197.
55 J. R. Martin, P. Patil, F. Yu, M. K. Gupta and C. L. Duvall, *Biomaterials*, 2020, **263**, 120377.
56 Z. Li, T. Zhao, J. Ding, H. Gu, Q. Wang, Y. Wang, D. Zhang and C. Gao, *Bioact. Mater.*, 2023, **19**, 550–568.
57 Z. An, L. Zhang, Y. Liu, H. Zhao, Y. Zhang, Y. Cao, Y. Zhang and R. Pei, *Biomater. Sci.*, 2022, **10**, 100–113.
58 L. Huang, J. Wang, L. Kong, X. Wang, Q. Li, L. Zhang, J. Shi, J. Duan and H. Mu, *Int. J. Biol. Macromol.*, 2022, **222**, 1476–1486.
59 S. Wu, H. Zhang, S. Wang, J. Sun, Y. Hu, H. Liu, J. Liu, X. Chen, F. Zhou, L. Bai, X. Wang and J. Su, *Mater. Horiz.*, 2023, **10**, 3507–3522.
60 J. Wang, Y. Yang, L. Huang, L. Kong, X. Wang, J. Shi, Y. Lü, H. Mu and J. Duan, *Int. J. Biol. Macromol.*, 2022, **219**, 1009–1020.
61 S. Liu, Q. Zhang, J. Yu, N. Shao, H. Lu, J. Guo, X. Qiu, D. Zhou and Y. Huang, *Adv. Healthcare Mater.*, 2020, **9**, 2000198.
62 J. Zhang, T. Tokatlian, J. Zhong, Q. K. T. Ng, M. Patterson, W. E. Lowry, S. T. Carmichael and T. Segura, *Adv. Mater.*, 2011, **23**, 5098–5103.
63 X. Huang, Y. Ye, J. Zhang, X. Zhang, H. Ma, Y. Zhang, X. Fu, J. Tang, N. Jiang, Y. Han, H. Liu and H. Chen, *ACS Appl. Mater. Interfaces*, 2022, **14**, 33756–33767.
64 F. Qian, Y. Han, Z. Han, D. Zhang, L. Zhang, G. Zhao, S. Li, G. Jin, R. Yu and H. Liu, *Biomaterials*, 2021, **270**, 120675.
65 M. G. Bezold, A. R. Hanna, B. R. Dollinger, P. Patil, F. Yu, C. L. Duvall and M. K. Gupta, *Adv. Funct. Mater.*, 2023, **33**, 2213368.
66 M. Regato-Herbella, I. Morhenn, D. Mantione, G. Pascuzzi, A. Gallastegui, A. B. Caribé dos Santos Valle, S. E. Moya, M. Criado-Gonzalez and D. Mecerreyes, *Chem. Mater.*, 2023, **36**, 1262–1272.
67 F. Li, X. Zhang, S. Hu, Z. Lv, J. Lv, W. Yu, X. Xu and D. Yang, *Chem. Mater.*, 2020, **32**, 2156–2165.
68 T. Sun, C. Zhu and J. Xu, *Soft Matter*, 2018, **14**, 921–926.
69 H. J. Jo, J.-H. Yang, A. I. Robby, G. Lee, E.-J. Jin and S. Y. Park, *Sens. Actuators, B*, 2023, **390**, 133945.
70 A. Shit, S. Park, Y. Lee, B. Ryplida, N. Morgan, Y. C. Jang, E.-J. Jin and S. Y. Park, *Acta Biomater.*, 2023, **171**, 406–416.
71 H. J. Jo, G.-B. Im, A. I. Robby, I. In, S. H. Bhang, A. Shit and S. Y. Park, *Chem. Eng. J.*, 2023, **455**, 140729.
72 W. Lu, X. Xu, L. Imbernon, J. Zhu, R. Hoogenboom, F. E. Du Prez and X. Pan, *Biomacromolecules*, 2020, **21**, 3308–3317.
73 C. Yang, C. Zhu, Y. Li, Z. Li, Z. Zhang, J. Xu, M. Chen, R. Li, S. Liu, Y. Wu, Z. Huang and C. Wu, *Front. Bioeng. Biotechnol.*, 2022, **10**, 912562.
74 X. Ding, M. Zang, Y. Zhang, Y. Chen, J. Du, A. Yan, J. Gu, Y. Li, S. Wei, J. Xu, H. Sun, J. Liu and S. Yu, *Acta Biomater.*, 2023, **167**, 182–194.
75 Y.-J. Jo, M. Gulfam, S.-H. Jo, Y.-S. Gal, C.-W. Oh, S.-H. Park and K. T. Lim, *Carbohydr. Polym.*, 2022, **286**, 119303.
76 Z. Zhou, Y. Liu, W. Li, Z. Zhao, X. Xia, J. Liu, Y. Deng, Y. Wu, X. Pan, F. He, H. Yang, W. Lu, Y. Xu and X. Zhu, *Adv. Healthcare Mater.*, 2023, **13**, 2302153.

77 E. Pezron, L. Leibler, A. Ricard, F. Lafuma and R. Audebert, *Macromolecules*, 2002, **22**, 1169–1174.
78 S. Kesavan and R. K. Prud'homme, *Macromolecules*, 2002, **25**, 2026–2032.
79 E. Pezron, A. Ricard, F. Lafuma and R. Audebert, *Macromolecules*, 2002, **21**, 1121–1125.
80 D. J. Power, A. B. Rodd, L. Paterson and D. V. Boger, *J. Rheol.*, 1998, **42**, 1021–1037.
81 S. W. Sinton, *Macromolecules*, 2002, **20**, 2430–2441.
82 G. F. S. Fernandes, W. A. Denny and J. L. Dos Santos, *Eur. J. Med. Chem.*, 2019, **179**, 791–804.
83 J. Lv, Z. Yang, C. Wang, J. Duan, L. Ren, G. Rong, Q. Feng, Y. Li and Y. Cheng, *J. Controlled Release*, 2023, **355**, 160–170.
84 W. Yang, X. Gao and B. Wang, *Med. Res. Rev.*, 2003, **23**, 346–368.
85 S. Biswas, J. Das, S. Barman, B. Rao Pinninti, T. K. Maiti and N. D. P. Singh, *ACS Appl. Mater. Interfaces*, 2017, **9**, 28180–28184.
86 A. Bedini, A. Fraternale, R. Crinelli, M. Mari, S. Bartolucci, L. Chiarantini and G. Spadoni, *Chem. Res. Toxicol.*, 2018, **32**, 100–112.
87 B. J. Graham, I. W. Windsor, B. Gold and R. T. Raines, *Proc. Natl. Acad. Sci. U. S. A.*, 2021, **118**, 13691118.
88 V. H. Deuel and H. Neukom, *Rapid Commun.*, 1949, **3**, 13–30.
89 M. Piest, X. Zhang, J. Trinidad and J. F. J. Engbersen, *Soft Matter*, 2011, **7**, 11111.
90 I. D. Robb and J. B. A. F. Smeulders, *Polymer*, 1997, **38**, 2165–2169.
91 M. H. Othman, Y. Ito and J. Akimoto, *ACS Appl. Polym. Mater.*, 2022, **4**, 5047–5055.
92 B. Lu, F. Lin, X. Jiang, J. Cheng, Q. Lu, J. Song, C. Chen and B. Huang, *ACS Sustainable Chem. Eng.*, 2016, **5**, 948–956.
93 J. Xu, D. Yang, W. Li, Y. Gao, H. Chen and H. Li, *Polymer*, 2011, **52**, 4268–4276.
94 V. Yesilyurt, M. J. Webber, E. A. Appel, C. Godwin, R. Langer and D. G. Anderson, *Adv. Mater.*, 2016, **28**, 86–91.
95 M. Bérubé, M. Dowlut and D. G. Hall, *J. Org. Chem.*, 2008, **73**, 6471–6479.
96 M. Dowlut and D. G. Hall, *J. Am. Chem. Soc.*, 2006, **128**, 4226–4227.
97 A. Adamczyk-Woźniak, K. M. Borys and A. Sporzyński, *Chem. Rev.*, 2015, **115**, 5224–5247.
98 D. Li, Y. Chen and Z. Liu, *Chem. Soc. Rev.*, 2015, **44**, 8097–8123.
99 A. Adamczyk-Woźniak, M. K. Cabaj, P. M. Dominiak, P. Gajowiec, B. Gierczyk, J. Lipok, Ł. Popenda, G. Schroeder, E. Tomecka, P. Urbański, D. Wieczorek and A. Sporzyński, *Bioorg. Chem.*, 2015, **60**, 130–135.
100 J. Chen, H. Zhu, J. Xia, Y. Zhu, C. Xia, Z. Hu, Y. Jin, J. Wang, Y. He, J. Dai and Z. Hu, *Adv. Sci.*, 2023, **10**, 2206306.
101 M. Li, X. Shi, B. Yang, J. Qin, X. Han, W. Peng, Y. He, H. Mao, D. Kong and Z. Gu, *Carbohydr. Polym.*, 2022, **296**, 119953.
102 H. Deuel, H. Neukom and F. Weber, *Nature*, 1948, **161**, 96–97.
103 L. Cruz, N. Mateus and V. de Freitas, *Carbohydr. Polym.*, 2022, **280**, 119029.
104 Y. Tezuka, *Prog. Polym. Sci.*, 1992, **17**, 471–514.
105 Y. Xia, R. Verduzco, R. H. Grubbs and J. A. Kornfield, *J. Am. Chem. Soc.*, 2008, **130**, 1735–1740.
106 R. Jerome, M. Henrioulle-Granville, B. Boutevin and J. J. Robin, *Prog. Polym. Sci.*, 1991, **16**, 837–906.
107 D. Khedaioui, C. Boisson, F. D'Agosto and D. Montarnal, *Angew. Chem., Int. Ed.*, 2019, **58**, 15883–15889.
108 S. Ge, S. Samanta, B. Li, G. P. Carden, P.-F. Cao and A. P. Sokolov, *ACS Nano*, 2022, **16**, 4746–4755.
109 B. Wu, C. Yang, Q. Xin, L. Kong, M. Eggersdorfer, J. Ruan, P. Zhao, J. Shan, K. Liu, D. Chen, D. A. Weitz and X. Gao, *Adv. Mater.*, 2021, **33**, 2102362.
110 D. Astruc, *Eur. J. Inorg. Chem.*, 2016, 6–29.
111 H. Gu, S. Mu, G. Qiu, X. Liu, L. Zhang, Y. Yuan and D. Astruc, *Coord. Chem. Rev.*, 2018, **364**, 51–85.
112 G. Saravanakumar, J. Kim and W. J. Kim, *Adv. Sci.*, 2017, **4**, 1600124.
113 C. Jia, I. M. Grace, P. Wang, A. Almeshal, Z. Huang, Y. Wang, P. Chen, L. Wang, J. Zhou, Z. Feng, Z. Zhao, Y. Huang, C. J. Lambert and X. Duan, *Chem*, 2020, **6**, 1172–1182.
114 M. G. Walawalkar, P. Pandey and R. Murugavel, *Angew. Chem., Int. Ed.*, 2021, **60**, 12632–12635.
115 T. Matsue, D. H. Evans, T. Osa and N. Kobayashi, *J. Am. Chem. Soc.*, 2002, **107**, 3411–3417.
116 M. Nakahata, Y. Takashima, A. Hashidzume and A. Harada, *Angew. Chem., Int. Ed.*, 2013, **52**, 5731–5735.
117 F. Li and T. Ito, *J. Am. Chem. Soc.*, 2013, **135**, 16260–16263.
118 C. S. Patrickios and T. K. Georgiou, *Curr. Opin. Colloid Interface Sci.*, 2003, **8**, 76–85.
119 M. Patenaude, N. M. B. Smeets and T. Hoare, *Macromol. Rapid Commun.*, 2014, **35**, 598–617.
120 M. J. Khan, J. Zhang and Q. Guo, *Chem. Eng. J.*, 2016, **301**, 92–102.
121 R. L. N. Hailes, A. M. Oliver, J. Gwyther, G. R. Whittell and I. Manners, *Chem. Soc. Rev.*, 2016, **45**, 5358–5407.
122 V. Bellas and M. Rehahn, *Angew. Chem., Int. Ed.*, 2007, **46**, 5082–5104.
123 X. Sui, M. A. Hempenius and G. J. Vancso, *J. Am. Chem. Soc.*, 2012, **134**, 4023–4025.
124 M. R. Rao and S.-S. Sun, *Langmuir*, 2013, **29**, 15146–15158.
125 H. Li, Y. Yang, F. Xu, T. Liang, H. Wen and W. Tian, *Chem. Commun.*, 2019, **55**, 271–285.
126 G. Zhao, Y. Wang, C. Wang, H. Lei, B. Yi and R. Tong, *Green Chem.*, 2022, **24**, 4041–4049.
127 Z. Zhai, W. Ouyang, Y. Yao, Y. Zhang, H. Zhang, F. Xu and C. Gao, *Bioact. Mater.*, 2022, **14**, 430–442.
128 P. Pei, C. Sun, W. Tao, J. Li, X. Yang and J. Wang, *Biomaterials*, 2019, **188**, 74–82.
129 B. Liu and S. Thayumanavan, *Cell Rep. Phys. Sci.*, 2020, **1**, 100271.
130 M. Criado-Gonzalez and D. Mecerreyes, *J. Mater. Chem. B*, 2022, **10**, 7206–7221.
131 D. Spitzer, L. L. Rodrigues, D. Straßburger, M. Mezger and P. Besenius, *Angew. Chem., Int. Ed.*, 2017, **56**, 15461–15465.

132 S. Zhu, S. Li, H. Escuin-Ordinas, R. Dimatteo, W. Xi, A. Ribas and T. Segura, *J. Controlled Release*, 2018, **282**, 156–165.
133 M. Bortoli, F. Zaccaria, M. Dalla Tiezza, M. Bruschi, C. Fonseca Guerra, F. M. Bickelhaupt and L. Orian, *Phys. Chem. Chem. Phys.*, 2018, **20**, 20874–20885.
134 X. Lu, G. Mestres, V. Singh, P. Effati, J.-F. Poon, L. Engman and M. Ott, *Antioxidants*, 2017, **6**, 13.
135 L. Wang, K. Zhu, W. Cao, C. Sun, C. Lu and H. Xu, *Polym. Chem.*, 2019, **10**, 2039–2046.
136 M. Ruck and F. Locherer, *Coord. Chem. Rev.*, 2015, **285**, 1–10.
137 Z. Wang, L. Guo, H. Xiao, H. Cong and S. Wang, *Mater. Horiz.*, 2020, **7**, 282–288.
138 F. Fan, S. Ji, C. Sun, C. Liu, Y. Yu, Y. Fu and H. Xu, *Angew. Chem., Int. Ed.*, 2018, **57**, 16426–16430.
139 J. Xu, T. Chu, T. Yu, N. Li, C. Wang, C. Li, Y. Zhang, H. Meng and G. Nie, *ACS Nano*, 2022, **16**, 13037–13048.
140 S. G. Kim, B. Ryplida, N. N. Giang, G. Lee, K. D. Lee and S. Y. Park, *Chem. Eng. J.*, 2021, **426**, 130880.
141 Y. Zhang, S. Tian, L. Huang, Y. Li, Y. Lu, H. Li, G. Chen, F. Meng, G. L. Liu, X. Yang, J. Tu, C. Sun and L. Luo, *Nat. Commun.*, 2022, **13**, 4553.
142 H. Li, J. Zhang, H. Xue, L. Li, X. Liu, L. Yang, Z. Gu, Y. Cheng, Y. Li and Q. Huang, *Mater. Horiz.*, 2023, **10**, 1789–1794.
143 H. Cao, J. Zhu, J. Zhang, L. Yang, X. Guo, R. Tian, H. Wu, Y. Li and Z. Gu, *Chem. Mater.*, 2023, **35**, 2191–2201.
144 P. Yang, T. Wang, J. Zhang, H. Zhang, W. Bai, G. Duan, W. Zhang, J. Wu, Z. Gu and Y. Li, *Sci. China: Chem.*, 2023, **66**, 1520–1528.
145 F. Zhu, J. Zhong, J. Hu, P. Yang, J. Zhang, M. Zhang, Y. Li and Z. Gu, *CCS Chem.*, 2023, **5**, 257–270.
146 H. Cao, L. Yang, R. Tian, H. Wu, Z. Gu and Y. Li, *Chem. Soc. Rev.*, 2022, **51**, 4175–4198.
147 Z. Li, G. Davidson-Rozenfeld, M. Vázquez-González, M. Fadeev, J. Zhang, H. Tian and I. Willner, *J. Am. Chem. Soc.*, 2018, **140**, 17691–17701.
148 Y. Hu and C. Fan, *Chem*, 2022, **8**, 1554–1566.
149 T. E. Brown and K. S. Anseth, *Chem. Soc. Rev.*, 2017, **46**, 6532–6552.
150 T. Ghosh and A. K. Das, *Coord. Chem. Rev.*, 2023, **488**, 215170.
151 C. M. Madl, S. C. Heilshorn and H. M. Blau, *Nature*, 2018, **557**, 335–342.
152 Z. Chen, Y. Chen, M. S. Hedenqvist, C. Chen, C. Cai, H. Li, H. Liu and J. Fu, *J. Mater. Chem. B*, 2021, **9**, 2561–2583.
153 Y. Lee, W. J. Song and J. Y. Sun, *Mater. Today Phys.*, 2020, **15**, 100258.
154 J. Tan, Z. Deng, C. Song, J. Xu, Y. Zhang, Y. Yu, J. Hu and S. Liu, *J. Am. Chem. Soc.*, 2021, **143**, 13738–13748.
155 K. A. Miller, E. G. Morado, S. R. Samanta, B. A. Walker, A. Z. Nelson, S. Sen, D. T. Tran, D. J. Whitaker, R. H. Ewoldt, P. V. Braun and S. C. Zimmerman, *J. Am. Chem. Soc.*, 2019, **141**, 2838–2842.
156 S. H. Lee, M. K. Gupta, J. B. Bang, H. Bae and H. J. Sung, *Adv. Healthcare Mater.*, 2013, **2**, 908–915.
157 I. Tokarev and S. Minko, *Adv. Funct. Mater.*, 2019, **30**, 1903478.
158 B. Xu, L. Zhao, W. Li, J. He and Y. M. Xie, *Compos. Struct.*, 2016, **149**, 134–144.
159 S. Bose, D. Ke, H. Sahasrabudhe and A. Bandyopadhyay, *Prog. Mater. Sci.*, 2018, **93**, 45–111.
160 Y. Yang, X. Song, X. Li, Z. Chen, C. Zhou, Q. Zhou and Y. Chen, *Adv. Mater.*, 2018, **30**, 1706539.
161 F. Calignano, D. Manfredi, E. P. Ambrosio, S. Biamino, M. Lombardi, E. Atzeni, A. Salmi, P. Minetola, L. Iuliano and P. Fino, *Proc. IEEE Inst. Electr. Electron Eng.*, 2017, **105**, 593–612.
162 Q. He, T. Tang, Y. Zeng, N. Iradukunda, B. Bethers, X. Li and Y. Yang, *Adv. Funct. Mater.*, 2023, **34**, 2309323.
163 S. Latthe, C. Terashima, K. Nakata and A. Fujishima, *Molecules*, 2014, **19**, 4256–4283.
164 B. Dean and B. Bhushan, *Philos. Trans. R. Soc., A*, 2010, **368**, 4775–4806.
165 H. Chen, P. Zhang, L. Zhang, H. Liu, Y. Jiang, D. Zhang, Z. Han and L. Jiang, *Nature*, 2016, **532**, 85–89.
166 Z. Chen, D. Zhao, B. Liu, G. Nian, X. Li, J. Yin, S. Qu and W. Yang, *Adv. Funct. Mater.*, 2019, **29**, 1900971.
167 W. Cao, S. Peng, Y. Yao, J. Xie, S. Li, C. Tu and C. Gao, *Acta Biomater.*, 2022, **152**, 60–73.
168 A. Kumar, S. Mandal, S. Barui, R. Vasireddi, U. Gbureck, M. Gelinsky and B. Basu, *Mater. Sci. Eng., R*, 2016, **103**, 1–39.
169 S. C. Ligon, R. Liska, J. Stampfl, M. Gurr and R. Mülhaupt, *Chem. Rev.*, 2017, **117**, 10212–10290.
170 H. Quan, T. Zhang, H. Xu, S. Luo, J. Nie and X. Zhu, *Bioact. Mater.*, 2020, **5**, 110–115.
171 Y.-L. Tsai, P. Theato, C.-F. Huang and S.-H. Hsu, *Appl. Mater. Today*, 2020, **20**, 100778.
172 M. Rumi and J. W. Perry, *Adv. Opt. Photonics*, 2010, **2**, 451.
173 S. Kawata, H.-B. Sun, T. Tanaka and K. Takada, *Nature*, 2001, **412**, 697–698.
174 M. P. Jeske, W. Zhang and M. Anthamatten, *Adv. Mater. Technol.*, 2022, **7**, 2101725.
175 C. K. W. Lee, Y. Pan, R. Yang, M. Kim and M. G. Li, *Top. Curr. Chem.*, 2023, **381**, 18.
176 M. Jalaal, S. Li, M. Klein Schaarsberg, Y. Qin and D. Lohse, *Appl. Phys. Lett.*, 2019, **114**, 213703.
177 B. Mitu, A. Matei, M. Filipescu, A. Palla Papavlu, A. Bercea, T. Lippert and M. Dinescu, *J. Phys. D: Appl. Phys.*, 2017, **50**, 115601.
178 K. C. Hribar, P. Soman, J. Warner, P. Chung and S. Chen, *Lab Chip*, 2014, **14**, 268–275.
179 H. W. Ooi, C. Mota, A. T. ten Cate, A. Calore, L. Moroni and M. B. Baker, *Biomacromolecules*, 2018, **19**, 3390–3400.
180 R. Zhao, Y. Shen, X. Deng, Y. Tang, Z. Ge, D. Wang, Z. Xiong, Q. Fang, Z. Zhang, X. Li, X. Du, W. Lin, S. Zhao and G. Wang, *Composites, Part B*, 2023, **264**, 110909.
181 X. Li, B. Liu, B. Pei, J. Chen, D. Zhou, J. Peng, X. Zhang, W. Jia and T. Xu, *Chem. Rev.*, 2020, **120**, 10793–10833.
182 B. Zhang, L. Gao, L. Ma, Y. Luo, H. Yang and Z. Cui, *Engineering*, 2019, **5**, 777–794.

183 K. Arai, S. Iwanaga, H. Toda, C. Genci, Y. Nishiyama and M. Nakamura, *Biofabrication*, 2011, **3**, 034113.
184 A. Dufour, X. B. Gallostra, C. O'Keeffe, K. Eichholz, S. Von Euw, O. Garcia and D. J. Kelly, *Biomaterials*, 2022, **283**, 121405.
185 M. Cirelli, J. Hao, T. C. Bor, J. Duvigneau, N. Benson, R. Akkerman, M. A. Hempenius and G. J. Vancso, *ACS Appl. Mater. Interfaces*, 2019, **11**, 37060–37068.
186 M. Kainz, S. Haudum, E. Guillén, O. Brüggemann, R. Höller, H. Frommwald, T. Dehne, M. Sittinger, D. Tupe, Z. Major, G. Stubauer, T. Griesser and I. Teasdale, *Macromol. Mater. Eng.*, 2024, **309**, 2400028.
187 D. Ahn, L. M. Stevens, K. Zhou and Z. A. Page, *ACS Cent. Sci.*, 2020, **6**, 1555–1563.
188 K. S. Lim, R. Levato, P. F. Costa, M. D. Castilho, C. R. Alcala-Orozco, K. M. A. van Dorenmalen, F. P. W. Melchels, D. Gawlitta, G. J. Hooper, J. Malda and T. B. F. Woodfield, *Biofabrication*, 2018, **10**, 034101.
189 J.-F. Xing, M.-L. Zheng and X.-M. Duan, *Chem. Soc. Rev.*, 2015, **44**, 5031–5039.
190 W. Ouyang, X. Xu, W. Lu, N. Zhao, F. Han and S.-C. Chen, *Nat. Commun.*, 2023, **14**, 1716.
191 Q. Geng, D. Wang, P. Chen and S.-C. Chen, *Nat. Commun.*, 2019, **10**, 2179.
192 J. R. Tumbleston, D. Shirvanyants, N. Ermoshkin, R. Janusziewicz, A. R. Johnson, D. Kelly, K. Chen, R. Pinschmidt, J. P. Rolland, A. Ermoshkin, E. T. Samulski and J. M. DeSimone, *Science*, 2015, **347**, 1349–1352.
193 G. Lipkowitz, T. Samuelsen, K. Hsiao, B. Lee, M. T. Dulay, I. Coates, H. Lin, W. Pan, G. Toth, L. Tate, E. S. G. Shaqfeh and J. M. DeSimone, *Sci. Adv.*, 2022, **8**, 1–11.
194 T. Wang, J. W. Chen, Z. Q. Li and P. Y. Wan, *J. Photochem. Photobiol., A*, 2007, **187**, 389–394.
195 E. Faggi, C. Gascó, J. Aguilera, G. Guirado, S. Ortego, R. Sáez, F. Pujol, J. Marquet, J. Hernando and R. M. Sebastián, *Macromolecules*, 2019, **52**, 5602–5610.
196 Y. Yamaguchi and C. Kutal, *Macromolecules*, 2000, **33**, 1152–1156.
197 F. Dumur, *Eur. Polym. J.*, 2021, **147**, 110328.
198 L. Kong, R. Bhosale and G. R. Ziegler, *Food Res. Int.*, 2018, **105**, 446–452.
199 S. Zhang, H. Zhang, Z. Xu, M. Wu, W. Xia and W. Zhang, *Ind. Crops Prod.*, 2017, **95**, 60–65.
200 C. Deng, C. Cao, Y. Zhang, J. Hu, Y. Gong, M. Zheng and Y. Zhou, *Food Hydrocolloids*, 2022, **123**, 107013.
201 W. Zhang, M. Chen and G. Diao, *Electrochim. Acta*, 2011, **56**, 5129–5136.
202 L. Strohmeier, H. Frommwald and S. Schlögl, *RSC Adv.*, 2020, **10**, 23607–23614.
203 C. Yu, K. L. Miller, J. Schimelman, P. Wang, W. Zhu, X. Ma, M. Tang, S. You, D. Lakshmipathy, F. He and S. Chen, *Biomaterials*, 2020, **258**, 120294.
204 T. V. Neumann and M. D. Dickey, *Adv. Mater. Technol.*, 2020, **5**, 2000070.
205 J. E. Smay, J. Cesarano and J. A. Lewis, *Langmuir*, 2002, **18**, 5429–5437.
206 M. A. S. R. Saadi, A. Maguire, N. T. Pottackal, M. S. H. Thakur, M. M. Ikram, A. J. Hart, P. M. Ajayan and M. M. Rahman, *Adv. Mater.*, 2022, **34**, 2108855.
207 Q. Feng, D. Li, Q. Li, H. Li, Z. Wang, S. Zhu, Z. Lin, X. Cao and H. Dong, *ACS Appl. Mater. Interfaces*, 2022, **14**, 15653–15666.
208 M. O. Saed, C. P. Ambulo, H. Kim, R. De, V. Raval, K. Searles, D. A. Siddiqui, J. M. O. Cue, M. C. Stefan, M. R. Shankar and T. H. Ware, *Adv. Funct. Mater.*, 2018, **29**, 1806412.
209 T. Xu, H. Kincaid, A. Atala and J. J. Yoo, *J. Manuf. Sci. Eng.*, 2008, **130**, 021017.
210 C. W. Visser, R. Pohl, C. Sun, G.-W. Römer, B. Huis in't Veld and D. Lohse, *Adv. Mater.*, 2015, **27**, 4087–4092.
211 Z. Ur Rehman, F. Yang, M. Wang and T. Zhu, *Opt. Laser Technol.*, 2023, **160**, 109065.
212 S.-Y. Liang, Y.-F. Liu, Z.-K. Ji, S.-Y. Wang, H. Xia and H.-B. Sun, *Nano Lett.*, 2023, **23**, 3769–3774.
213 S.-Y. Liang, Y.-F. Liu, Z.-K. Ji, H. Xia and H.-B. Sun, *Chem. Eng. J.*, 2023, **466**, 143121.
214 N. Bakhtiari, S. Azizian and B. Jaleh, *J. Colloid Interface Sci.*, 2022, **625**, 383–396.
215 T. Jungst, W. Smolan, K. Schacht, T. Scheibel and J. Groll, *Chem. Rev.*, 2015, **116**, 1496–1539.
216 V. L. Workman, L. B. Tezera, P. T. Elkington and S. N. Jayasinghe, *Adv. Funct. Mater.*, 2014, **24**, 2648–2657.
217 R. E. Saunders and B. Derby, *Int. Mater. Rev.*, 2014, **59**, 430–448.
218 T. Boland, X. Tao, B. J. Damon, B. Manley, P. Kesari, S. Jalota and S. Bhaduri, *Mater. Sci. Eng., C*, 2007, **27**, 372–376.
219 T. Xu, C. Baicu, M. Aho, M. Zile and T. Boland, *Biofabrication*, 2009, **1**, 035001.
220 S.-X. Chen, J. Zhang, F. Xue, W. Liu, Y. Kuang, B. Gu, S. Song and H. Chen, *Bioact. Mater.*, 2023, **21**, 86–96.
221 B. Qiao, J. Wang, L. Qiao, A. Maleki, Y. Liang and B. Guo, *Regener. Biomater.*, 2024, **11**, rbad110.
222 Y. Zhu, Y. Matsumura, M. Velayutham, L. M. Foley, T. K. Hitchens and W. R. Wagner, *Biomaterials*, 2018, **177**, 98–112.
223 D. Zhao, Q. Zhou, K. Yang, H. Yang, Q. Tang and X. Zhang, *Macromol. Chem. Phys.*, 2019, **220**, 1900106.
224 B. Hu, Z. Lian, Z. Zhou, L. Shi and Z. Yu, *ACS Appl. Bio Mater.*, 2020, **3**, 5529–5551.
225 G. S. Han and D. W. Domaille, *J. Mater. Chem. B*, 2022, **10**, 6263–6278.
226 J. G. Powers, C. Higham, K. Broussard and T. J. Phillips, *J. Am. Acad. Dermatol.*, 2016, **74**, 607–625.
227 V. Falanga, *Lancet*, 2005, **366**, 1736–1743.
228 K. Rahim, S. Saleha, X. Zhu, L. Huo, A. Basit and O. L. Franco, *Microb. Ecol.*, 2016, **73**, 710–721.
229 X. Cheng, L. Li, L. Yang, Q. Huang, Y. Li and Y. Cheng, *Adv. Funct. Mater.*, 2022, **32**, 2206201.
230 V. Falanga, R. R. Isseroff, A. M. Soulika, M. Romanelli, D. Margolis, S. Kapp, M. Granick and K. Harding, *Nat. Rev. Dis. Primers*, 2022, **8**, 50.

231 H. Zhang, C. Huang, J. Zhang, C. Wang, T. Wang, S. Shi, Z. Gu and Y. Li, *Giant*, 2022, **12**, 100120.
232 W. Chengwei, L. Yihao, Y. Xiaoxiao, L. Wentao, Z. Xianhao, R. Ya, Z. Changru, Y. Han, K. Weiqing, W. Jinwu and N. Haoyi, *Chem. Eng. J.*, 2022, **450**, 138077.
233 W. Zhao, X. Zhang, R. Zhang, K. Zhang, Y. Li and F.-J. Xu, *ACS Appl. Mater. Interfaces*, 2020, **12**, 56898–56907.
234 J. P. Brown, S. Couillard-Després, C. M. Cooper-Kuhn, J. Winkler, L. Aigner and H. G. Kuhn, *J. Comp. Neurol.*, 2003, **467**, 1–10.
235 V. P. Torchilin, *Nat. Rev. Drug Discovery*, 2014, **13**, 813–827.
236 M. J. Mitchell, M. M. Billingsley, R. M. Haley, M. E. Wechsler, N. A. Peppas and R. Langer, *Nat. Rev. Drug Discovery*, 2020, **20**, 101–124.
237 K. M. Tsoi, S. A. MacParland, X.-Z. Ma, V. N. Spetzler, J. Echeverri, B. Ouyang, S. M. Fadel, E. A. Sykes, N. Goldaracena, J. M. Kaths, J. B. Conneely, B. A. Alman, M. Selzner, M. A. Ostrowski, O. A. Adeyi, A. Zilman, I. D. McGilvray and W. C. W. Chan, *Nat. Mater.*, 2016, **15**, 1212–1221.
238 W. Kim, N. K. Ly, Y. He, Y. Li, Z. Yuan and Y. Yeo, *Adv. Drug Delivery Rev.*, 2023, **192**, 114635.
239 A. Stubelius, W. Sheng, S. Lee, J. Olejniczak, M. Guma and A. Almutairi, *Small*, 2018, **14**, 1800703.
240 L. Roth, E. C. Wendling, C. N. Coleman, D. A. Pistenmaa and D. M. O'Brien, *Lancet*, 2019, **393**, 983–984.
241 M. Norouzi, B. Nazari and D. W. Miller, *Drug Discovery Today*, 2016, **21**, 1835–1849.
242 Z. Dai, Q. Zhang, X. Li, Q. Chen, J. Chen, M. Wang and H. Chen, *Mater. Today*, 2023, **65**, 62–77.
243 M. Wang, Q. Hu, J. Huang, F. Zhang, Z. Yao, S. Shao, X. Zhao and T. Liang, *Adv. Healthcare Mater.*, 2023, **12**, 2203264.
244 M. D. Samsky, D. A. Morrow, A. G. Proudfoot, J. S. Hochman, H. Thiele and S. V. Rao, *JAMA*, 2021, **326**, 1840.
245 S. B. Seif-Naraghi, J. M. Singelyn, M. A. Salvatore, K. G. Osborn, J. J. Wang, U. Sampat, O. L. Kwan, G. M. Strachan, J. Wong, P. J. Schup-Magoffin, R. L. Braden, K. Bartels, J. A. DeQuach, M. Preul, A. M. Kinsey, A. N. DeMaria, N. Dib and K. L. Christman, *Sci. Transl. Med.*, 2013, **5**, 173ra125.
246 Z. Li, D. Zhu, Q. Hui, J. Bi, B. Yu, Z. Huang, S. Hu, Z. Wang, T. Caranasos, J. Rossi, X. Li, K. Cheng and X. Wang, *Adv. Funct. Mater.*, 2021, **31**, 2004377.
247 L. A. Liotta and E. Kohn, *Nature*, 2004, **430**, 973–974.
248 N. N. Ng and A. S. Thakor, *Sci. Transl. Med.*, 2020, **12**, eaba4564.
249 T. A. Rando and F. Ambrosio, *Cell Stem Cell*, 2018, **22**, 306–309.
250 L. Bacakova, J. Zarubova, M. Travnickova, J. Musilkova, J. Pajorova, P. Slepicka, N. S. Kasalkova, V. Svorcik, Z. Kolska, H. Motarjemi and M. Molitor, *Biotechnol. Adv.*, 2018, **36**, 1111–1126.
251 T. Yuan, T. Wang, J. Zhang, P. Liu, J. Xu, Z. Gu, J. Xu and Y. Li, *ACS Nano*, 2023, **17**, 18562–18575.
252 X. Li, K. Xu, Y. He, B. Tao, K. Li, C. Lin, J. Hu, J. Wu, Y. Wu, S. Liu, P. Liu, H. Wang and K. Cai, *Biomaterials*, 2022, **287**, 121683.
253 Z. Liu, Y. Faraj, X. J. Ju, W. Wang, R. Xie and L. Y. Chu, *J. Polym. Sci., Part B: Polym. Phys.*, 2018, **56**, 1306–1313.
254 S. Naficy, H. R. Brown, J. M. Razal, G. M. Spinks and P. G. Whitten, *Aust. J. Chem.*, 2011, **64**, 1007.
255 L.-W. Xia, R. Xie, X.-J. Ju, W. Wang, Q. Chen and L.-Y. Chu, *Nat. Commun.*, 2013, **4**, 2226.
256 C.-L. Mou, X.-J. Ju, L. Zhang, R. Xie, W. Wang, N.-N. Deng, J. Wei, Q. Chen and L.-Y. Chu, *Langmuir*, 2014, **30**, 1455–1464.
257 K. Haraguchi, *Polym. J.*, 2011, **43**, 223–241.
258 M. Kanduč, W. K. Kim, R. Roa and J. Dzubiella, *Macromolecules*, 2018, **51**, 4853–4864.
259 J. Liang and B. Liu, *Bioeng. Transl. Med.*, 2016, **1**, 239–251.

